AIP | Journal of Applied Physics

Prediction of probabilistic ignition behavior of polymer-bonded explosives from microstructural stochasticity

A. Barua, S. Kim, Y. Horie, and M. Zhou

Citation: J. Appl. Phys. **113**, 184907 (2013); doi: 10.1063/1.4804251
View online: http://dx.doi.org/10.1063/1.4804251
View Table of Contents: http://jap.aip.org/resource/1/JAPIAU/v113/i18
Published by the American Institute of Physics.

JOURNAL OF APPLIED PHYSICS **113**, 184907 (2013)

Prediction of probabilistic ignition behavior of polymer-bonded explosives from microstructural stochasticity

A. Barua,[1] S. Kim,[1] Y. Horie,[2] and M. Zhou[1]
[1]*The George W. Woodruff School of Mechanical Engineering, School of Materials Science and Engineering, Georgia Institute of Technology, Atlanta, Georgia 30332-0405, USA*
[2]*Air Force Research Lab, Munitions Directorate, 2306 Perimeter Road, Eglin AFB, Florida 32542, USA*

(Received 17 March 2013; accepted 22 April 2013; published online 10 May 2013)

Random variations in constituent properties, constituent distribution, microstructural morphology, and loading cause the ignition of explosives to be inherently stochastic. An approach is developed to computationally predict and quantify the stochasticity of the ignition process in polymer-bonded explosives (PBXs) under impact loading. The method, the computational equivalent of carrying out multiple experiments under the same conditions, involves subjecting sets of statistically similar microstructure samples to identical overall loading and characterizing the statistical distribution of the ignition response of the samples. Specific quantities predicted based on basic material properties and microstructure attributes include the critical time to ignition at given load intensity and the critical impact velocity below which no ignition occurs. The analyses carried out focus on the influence of random microstructure geometry variations on the critical time to ignition at given load intensity and the critical impact velocity below which no ignition occurs. Results show that the probability distribution of the time to criticality (t_c) follows the Weibull distribution. This probability distribution is quantified as a function of microstructural attributes including grain volume fraction, grain size, specific binder-grain interface area, and the stochastic variations of these attributes. The relations reveal that the specific binder-grain interface area and its stochastic variation have the most influence on the critical time to ignition and the critical impact velocity below which no ignition is observed. For a PBX with 95% octahydro-1,3,5,7-tetranitro-1,3,5,7-tetrazocine content, the computationally predicted minimum impact velocity for ignition is in the range of 54–63 ms^{-1} depending on microstructure. This range is comparable to values measured experimentally for PBX9501 (53 ms^{-1} by Chidester *et al.*, "Low amplitude impact testing and analysis of pristine and aged solid high explosives," in Eleventh (International) Symposium on Detonation, ONR (1998), 33300. 60–84 ms^{-1} by Gruau *et al.*, "Ignition of a confined high explosive under low velocity impact," Int. J. Impact Eng. **36**, 537–550 (2009)). © *2013 AIP Publishing LLC*. [http://dx.doi.org/10.1063/1.4804251]

I. INTRODUCTION

Solid high explosives such as HMX (Octahydro-1,3,5,7-tetranitro-1,3,5,7-tetrazocine) and RDX (1,3,5-trinitroperhydro-1,3,5-triazine) have high energy densities on the order of 1 $kcal \cdot g^{-1}$. They are powerful sources of energy for propulsion as well as civil and military applications. Under ambient conditions, these materials release energy relatively slowly. However, their combustion can result in catastrophic detonations that propagate at speeds on the order of 7–9 $km \cdot s^{-1}$. During such a detonation process, the release rate of energy is known to be on the order of 100 $GW \cdot cm^{-2}$ at the detonation front. As a reference, the current total electric generating capacity of the United States is on the order of 400 GW.[3,4] Thus, an accidental detonation of these explosives (or even near detonation) could result in catastrophic tragedies. Unfortunately, history is full of events that cost not only huge monetary and materials losses but also human lives. Tragic accidents are a good motivator for research in the safety (safe handling and use) of explosives.

However, as remarked by Asay,[4] "the problem is that with all of the study and the thousands of years of experience, we still cannot predict with any precision, in general, what will happen to an explosive if we hit it, heat it, drag it, drop it, or do anything else outside of its design envelop." What is worse, the design envelop is "historically rooted in test protocols used in the qualification of the material that address its performance as well as safety and handling characteristics."[5] Hence, many different relative safety tests must be run to improve the probability that all detonation scenarios have been identified. The tests include a variety of stimuli to energy release, both intentional and accidental, that are mechanical, thermal, electrical, and shock-wave-induced in nature. The accidental detonation of solid high explosives is a hazard that depends on the sensitivity of the materials to these stimuli with regard to the initiation of chemical reaction. Other hazards include chemical instability and toxicity. The focus of this paper relates to the sensitivity to impact-induced mechanical insult.

As underlined by Asay[4] above, the sensitivity of solid high explosives is a difficult, if not intractable, subject. There have been efforts to move the development of these materials from empiricism based on protocols to design science based on modeling and simulation that capture relevant physics. The trend is to relate design, synthesis, test and evaluation to control, and ensure functionality.[5] These efforts are stimulated by progress in experimental techniques,[6,52] theory,[4] numerical models,[7–11] and computing tools (high

performance computing). In this paper, impact loading in the non-shock regime is of particular interest. Attention is specially focused on understanding the initiation of reaction in terms of hotspot dynamics at the grain scale and the stochasticity in macroscopic behavior. The latter feature, that is inherent in heterogeneous explosives, results from the interaction of deformation waves with material microstructure. The ultimate goal of this research is to elucidate some of the fundamental questions raised in Ref. 4 and provide a computational framework for helping shift the development of solid high explosives from empirical process to integrated materials design science.[12] Specifically, some of the questions we will attempt to address are as follows:

(1) Is there a way to characterize the complex pattern of the behavior of explosives related to ignition sensitivity? Is the probabilistic language used for the failure of structural composites relevant for solid high explosives?
(2) Is there a characteristic scale of sensitivity at the grain level just as the characteristic scale at the molecular scale (see, e.g., Ref. 13)? Are past failures of finding such a scale from macroscopic tests rooted in the fact that these tests are not controlled at the grain level (e.g., variations in particle morphology, size distribution, defects, and impurities are not controlled)?
(3) Is there a threshold impact velocity above which an explosive will always detonate? It is likely that this question needs to be couched in a probabilistic language because of the inherent heterogeneity of explosive composites and the stochastic nature of their properties.

The use of statistical or probabilistic approaches to understanding chemical initiation dates back many years. Cochran was the first to introduce a statistical treatment of heterogeneities that influence shock initiation.[14] He carried out a preliminary calculation for PBX 9404 and indicated that, with refinement, the model can duplicate the success of the ignition and growth model.[15] Indeed, this approach was expanded to include local thermo-chemical reactions and showed that the model has the capability to capture essential features of (1) shock-induced ignition and growth leading up to detonation, (2) quenching, and (3) curved detonation.[16,17]

Recently, Nichols and Tarver[18] adopted a different route for extending the Cochran approach by introducing a statistical hotspot model in ALE3D which considers the effects of initial shock pressure and density of hotspots on the shock-induced initiation of polymer-bonded explosives (PBXs). Hill and Zimmermann[19] reduced this model into an analytically solvable problem. Baras *et al.*[20] explored a stochastic description of exothermic reactions leading to adiabatic explosion. Chemical reactions are modeled as a Markovian birth and death process that bears some resemblance to the approach by Nichols and Tarver.[18] Browning and Scammon[21] developed an analytical threshold condition by combining heat conduction with chemical kinetics and sliding friction in both one and two dimensions. Gruau *et al.*[2] expanded on the work by Browning on frictional heating. Using a concrete-like constitutive law for PBX with pressure-dependent plasticity, the authors were able to replicate the dot- or ring-shaped ignition seen in the Steven test.[45]

Baer and his colleagues[22] have pursued a PDF (probability density function) approach in the manner of turbulent flow modeling. Although the mathematics is elegant, it is not yet clear how the solutions can be related to explosive sensitivity in terms of inherent material heterogeneities. The separation of cause and effect is itself an unfinished research topic.

Terao[23] proposed a general approach for describing a variety of irreversible phenomena in a stochastic framework. The basic tenant is that fluctuations inherent in irreversible processes are not random events but are governed by the probability of the irreversible process passing the minimum entropy state. He showed that the average ignition time is related to activation energies[24–26] and deduced a unified picture of experimental measurements through a stochastic analysis. Using this approach, Gilbert and Gonthier[27] analyzed the deformation-induced ignition response of granular HMX, by combining the temperature fields obtained from inert mesoscale calculations with a temperature threshold of 600 K to determine hotspots which have thermal runaway. One concern regarding this analysis is that it considers only the temperature and not the combined effect of the size and temperature of hotspots, which is necessary for thermal runaway as shown in Tarver *et al.*[28] Another inherent problem with this approach is that it does not capture the stochastic response arising out of variations in constituent properties, load condition, microstructural morphology, and constituent distribution.

The immediate goal of the current research is to develop a framework for computationally predicting and quantifying the stochasticity of the ignition process in PBXs under impact loading. The focus is on the influence of microstructure geometry on the critical time to ignition and the critical impact velocity below which no ignition occurs. This is accomplished by accounting for three key issues. The first issue involves the analysis of thermal and mechanical responses of heterogeneous energetic materials at the micro-level. This analysis uses a recently developed capability based on the cohesive finite element method (CFEM).[11,29–31] The second issue has been detailed in Barua *et al.*[32] and concerns hotspot generation and ignition criteria for the thermal runaway of critical hotspots. The third issue, the primary subject of this paper, is the effect of random fluctuations in the microstructure geometry on the ignition response of PBX.

This issue is handled by subjecting sets of statistically similar microstructure samples to identical overall loading and characterizing the statistical distribution of the ignition responses of the samples. The quantification of this distribution as a function of microstructural attributes including grain volume fraction, grain size, specific grain-binder interface area, and the stochastic variations of these attributes is used to identify the microstructural attributes which play dominant roles in determining the ignition behavior of these materials. This analysis will help establish microstructure-performance maps for developing PBXs with tailored attributes.

II. STOCHASTIC BEHAVIOR ANALYZED

In this analysis, we focus on the stochasticity arising out of variations in microstructure geometry. Our approach to assess the sensitivity of explosives combines the

deterministic analysis using the micromechanical CFEM[11] and a stochastic treatment of the numerical results from a large number of microstructure instantiations. This is essentially the computational equivalent of carrying out a large number of experiments under the same conditions.

In the following analyses each sample represents a single microstructure instantiation. The method by which microstructures are generated is discussed in Sec. II A. A "statistically similar set" consists of a number of microstructures having the same overall packing density η, average grain size d, and grain size distribution. In addition to these attributes, the analysis also considers sets of microstructures having specified variations in the specific surface area of the grains (ΔS_v) and the grain size distribution. Specifically, the sensitivity of a particular PBX composition is evaluated by performing numerical "experiments" on multiple instantiations of statistically similar microstructures.

The goal of this approach is to ascertain the dominant trends which relate microstructure to ignition sensitivity. Specifically, the variations at the microstructure level are related to the variations in the probability of ignition. The details of the materials analyzed and the ignition criteria used are outlined in Secs. II A–II C.

A. Material

This paper focuses on PBXs which have two-phase microstructures consisting of HMX grains and an Estane binder. Calculations are performed on computationally generated microstructures. However, the approach is equally applicable to scanned real microstructures as shown in Ref. 11. The benefits of using computationally generated microstructures here are (1) large (>1000) numbers of sample instantiations can be obtained and (2) sets of samples with attributes that conform to prescribed statistical distribution functions, averages and random fluctuations can be obtained in a controlled manner. These considerations are especially important for the current analyses, as will become clearer later.

The microstructures generated have multifaceted grains with monomodal and bimodal distributions of sizes. The microstructures having monomodal size distributions are generated using the Voronoi tessellation function. This is a geometric method that allows us to define a statistical sample space in a relatively straightforward way. The packing density is varied by properly altering the average thickness of the binder phase between neighboring grains. The mean grain size is 250 μm, with a standard deviation of 90 μm. Note that in the generation of microstructures using Voronoi tessellation, the energetic granules are effectively "grown" in place, subject to spatial constraint, whereas in actual PBXs, the grains are grown in solution and pressed or cast to the desired density and composition. In Ref. 11, a limited study was carried out on the shape and size of granules generated using Voronoi tessellation. It is found that the effect of the method on shape is on the same order as that on grain size distribution. Microstructures generated using particles from digitally scanned real material microstructures have been used by Barua *et al.*[11,29–31] and may be used in the future.

To generate microstructures with bimodal size distributions, a grain library is used. This library consists of grains extracted from monomodal microstructures which are generated using the Voronoi tessellation method. To achieve higher packing densities, the larger grains ($d > 250\ \mu$m) are initially placed at random locations up to a specified volume fraction (e.g., $\eta = 0.40$). Subsequently, smaller grains ($d < 100\ \mu$m) are placed between the larger grains, until the desired volume fraction ($\eta = 0.70$–0.84) is reached. The time required to generate a micrograph increases with the desired packing density. To reduce the time required in generating micrographs with high packing densities ($\eta > 0.80$), a random shuffling algorithm is employed. Specifically, if a grain cannot be placed in the domain, the locations of the existing grains are randomly altered until an empty region can be found for that particular grain. Naturally, such a method cannot be used indefinitely, since beyond a certain packing density, grains of a particular size can no longer be accommodated. This method allows relatively high packing densities (up to 0.84) to be achieved. For the bimodal distributions, the two mean grain sizes are ~61 μm and ~287 μm. The average standard deviations for the smaller and larger sizes are 20.53 μm and 40.6 μm, respectively.

A total of six different microstructural configurations are considered. The volume fraction is in the range of $\eta = 0.70$–0.90, involving both the monomodal and bimodal grain size distributions. One representative micrograph is shown for each of the six configurations in Figs. 1(a)–1(f). The microstructures analyzed, along with their attributes are listed in Table I. The grain size distributions for the microstructures in Fig. 1 are shown in Fig. 2. For each microstructural setting listed in Table I, up to thirty statistically identical samples (random instantiations) are generated. To

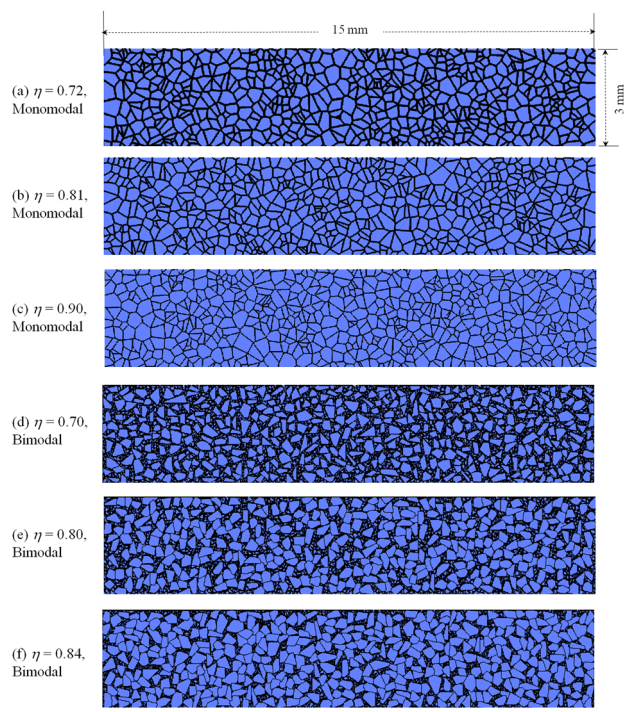

FIG. 1. Microstructures with different grain volume fractions ($\eta = 0.70$–0.90) and grain size distributions (monomodal and bimodal).

TABLE I. Microstructures analyzed.

Microstructure	Grain volume fraction (η)	Average grain Size (μm)	Standard deviation (μm)	Average specific surface area, S_v (mm^{-1})
PBX – Mono modal	0.72	235.1	87.4	15.65
	0.81	250.1	90.0	16.38
	0.90	264.3	92.1	17.37
PBX – Bimodal	0.70	64.3–251.2	19.7–45.3	25.26
	0.80	61.0–301.7	21.4–31.6	21.06
	0.84	59.6–307.5	20.5–44.9	18.00

illustrate the random variations in microstructure geometry within one particular set, Figure 3 shows 10 microstructures having the same packing density of $\eta = 0.81$ and monomodal grain size distribution. Further details of the statistical approach of analysis are provided in Sec. II C.

The variations of grain size distribution within a particular set of microstructures with otherwise similar attributes (volume fraction, average grain size) can also affect the variability in the ignition response. For this purpose, two additional sets of microstructures are generated with large and small variations in grain size distribution. Figures 4(a)–4(d) quantify the distributions of mean grain size and the distributions of the variations in the grain size relative to the mean grain sizes for these two sets of microstructures. The volume fraction of the grains is $\eta = 0.81$ and the size distribution is monomodal.

The microstructures are meshed using linear triangular elements arranged in a cross-triangular fashion. Sufficient

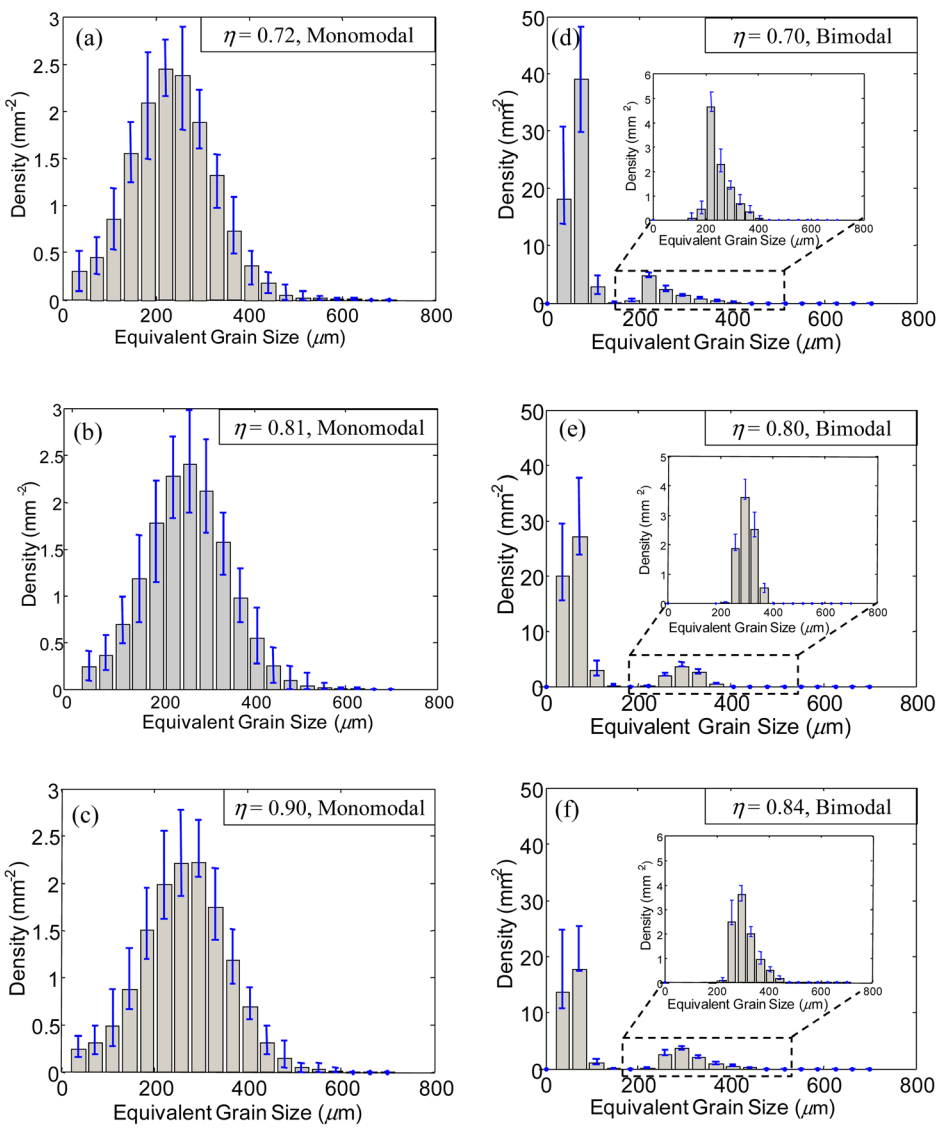

FIG. 2. Grain size distributions for the microstructures shown in Fig. 1.

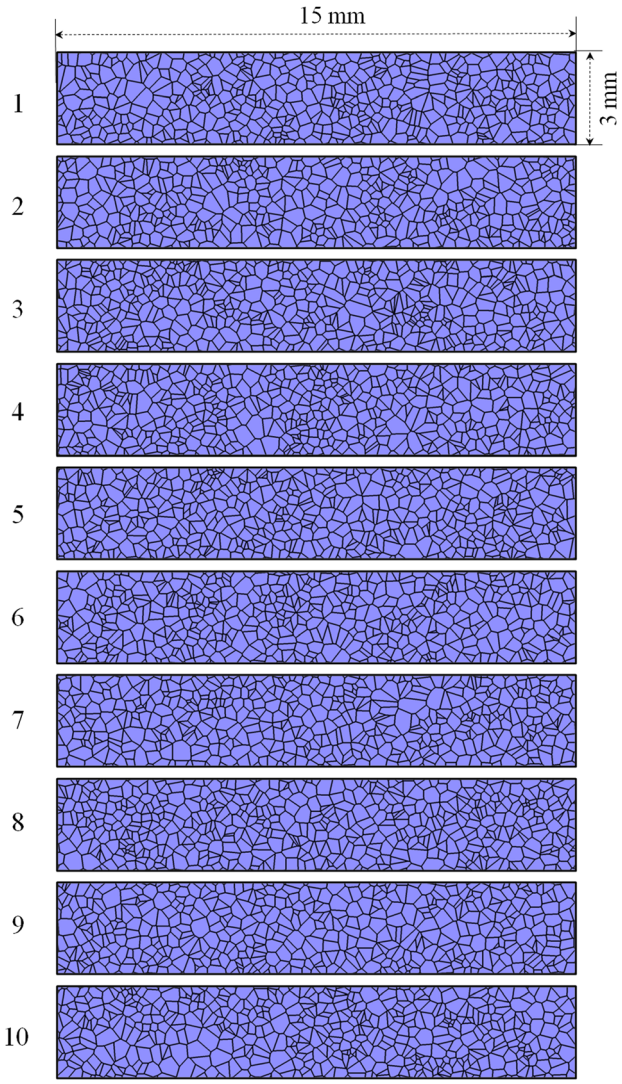

FIG. 3. Multiple instantiations of microstructures having a grain volume fraction of $\eta = 0.81$ and the monomodal size distribution.

mesh resolution is required to capture the stress and temperature distributions as well as microstructure heterogeneities. The microstructures are meshed using linear triangular elements arranged in a structured cross-triangular fashion. It should be pointed out that calculations are carried out using mesh sizes from 10 to 20 μm. As discussed in Ref. 32, the results converge as the mesh size is decreased beyond 15 μm. Specifically, the variation of hotspot size leads to a variation of time to criticality t_c of less than 5.0% for a 33% reduction in the mesh size from 15 to 10 μm, suggesting that the mesh resolution chosen (15 μm) is adequate for the purpose of the current study. Finite element sizes smaller than what is used may provide slightly better resolution of the hotspots, but also significantly increase calculation time.

B. Ignition criterion

A recently developed ignition criterion for establishing the ignition conditions of heterogeneous energetic materials under general conditions is used. This ignition criterion is discussed in detail in Ref. 32 and only a brief description is provided here.

This criterion links the hotspot size-temperature states in a loading event to the threshold size-temperature conditions of hotspots[28] which are regarded as materials properties. The criterion, along with the CFEM capability to quantify the thermal-mechanical behavior of energetic materials, allows the time to criticality (t_c), critical impact velocity (v) for ignition and critical input energy at ignition (E_c) to be determined as functions of material composition, microstructure, and loading conditions.[32]

Mathematically, this criterion provides a relationship between the size and temperature of critical hotspots as

$$d(T) \geq d_c(T), \tag{1}$$

where d is the diameter of the dominant hotspot resulting from a loading event whose interior temperatures are at or above temperature T and d_c is the minimal diameter of a hotspot required for thermal runaway at temperature T. The information regarding the right-hand side of Eq. (1) comes from Tarver *et al.*,[28] who performed chemical kinetics calculations to analyze the criticality issue for HMX and TATB explosives. The calculations consider multistep reaction mechanisms and the pressure and temperature dependence of reactants and products. We note that ignition is influenced by the duration of loading (transient effects) and that the chemical decomposition of energetic materials requires the hotspots to be above the temperature-size threshold for some length of time to complete. This process, while not the subject of study in this paper, should certainly be analyzed in the future. Here in this paper, the imposed loading (in the form of an imposed boundary velocity) is sustained for the complete duration of analysis, so that the time to criticality can be studied in a simple, clear, and well-defined setting.

To avoid the use of arbitrary size-temperature criteria in identifying hotspots, a recently developed scheme based on the radial distribution function (RDF) developed in Ref. 32 is used. This approach involves the use of a temperature threshold (ΔT_{thres}), which is of vital importance. At each time step, the microstructure is scanned for temperature increases above ΔT_{thres}. Areas with temperatures above the threshold are analyzed for hotspots. When different values for the temperature threshold are used, the distributions of the shapes and sizes of hotspots with temperature increases above the threshold can be characterized. Successively varying ΔT_{thres} values allow the characteristics of a temperature field to be fully analyzed. In particular, strategically chosen threshold temperature values allow hotspots of interest to be identified.

The left-hand side of Eq. (1) is obtained by analyzing the hotspot distributions from the CFEM calculations. To account for the variation of temperature within a hotspot (note that temperatures at different spatial locations within a hotspot are different and ΔT_{thres} is the lowest temperature at the periphery), the criterion of Tarver *et al.* is stated as a band of $\pm$ 10% about the mean value. A hotspot is considered to be critical when it crosses the lower threshold limit (90% of the average threshold). Taking into consideration the stochastic nature of arbitrary microstructures, we employ an approach to identify the time to criticality t_c measured

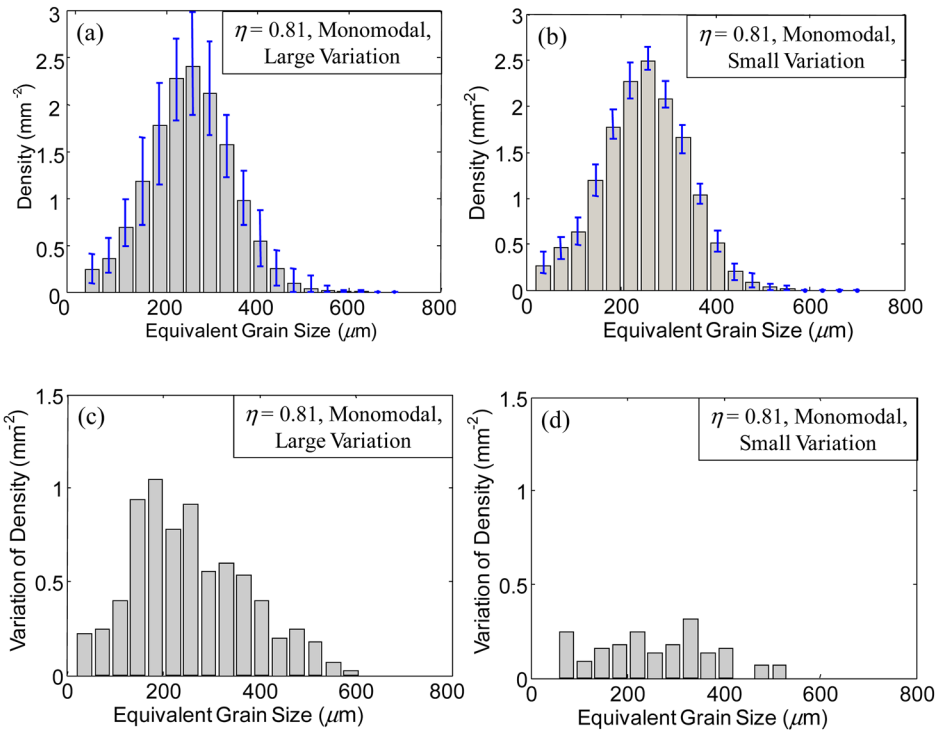

FIG. 4. Grain size distributions for microstructures having the same grain volume fraction of $\eta = 0.81$ with (a) large grain size distribution variations and (b) small grain size distribution variations about the mean grain size distribution. Quantification of the variations is in (c) and (d), respectively.

from the onset of dynamic loading. Specifically, instead of one single hotspot, criticality is regarded as being reached if the critical hotspot density in a specimen reaches a level equal to or greater than $0.22\,\mathrm{mm}^{-2}$. This level corresponds to 2 critical hotspots in a 3 mm square domain. It is important to point out that variations in the choice of this parameter do not significantly change the results. As discussed in Barua *et al.*,[32] for a change of critical hotspot density from 0.11 to $0.44\,\mathrm{mm}^{-2}$, the maximum variation in t_c is within 6% for a PBX microstructure having a packing density of 0.82 in several calculations with impact velocities between $v = 50$ and $250\,\mathrm{ms}^{-1}$. This shows that the value of the critical hotspot density chosen is quite reasonable and does not cause large changes in results. Although this treatment contains a degree of arbitrariness, it allows relative comparisons to be made when used consistently for difference cases.

C. Quantification of stochasticity

The stochastic nature of microstructural heterogeneities such as varying grain size and random constituent morphologies necessitates a statistical approach in the quantification of hotspot formation. This in turn requires an account of stochasticity in the application of the ignition criterion and hotspot threshold method described in Sec. II B. The analysis of hotspot criticality reflects such a probabilistic viewpoint.

To account for the stochastic variations in microstructures, sets of 10–50 microstructures with statistically similar attributes are constructed and used. The stochasticity analysis begins with running a fully dynamic thermomechanical impact response simulation and measuring the time to criticality for each sample in the microstructure sets. The different times to criticality in each set are taken together to quantify the stochastic variation in the behavior of the material with a particular attribute combination. The microstructural attributes considered are HMX volume fraction (η) which is often referred to as the packing density, grain size distribution (mean grain size δ and standard deviation σ), area of the interface between the HMX phase and the polymer binder per unit volume (S_v, often referred to as the specific interface area), and the statistical variations of these quantities among samples in each microstructure set. These quantities measure the stochastic variations in the microstructures and, along with the load intensity represented by the impact velocity (v), constitute the input to our statistical model. On the other hand, the times to criticality measure the stochastic variations in material behavior and represent the output in our statistical model. The output also includes the threshold impact velocity below which no ignition is observed (v_c) for a particular statistical microstructure configuration (Fig. 1).

Once an ensemble (or a set of microstructures) is defined, the distribution of the time to criticality can be uniquely determined for any given load intensity. For each set of microstructures having a given combination of statistically similar attributes, the time to criticality (t_c) is evaluated as a cumulative probability distribution. Naturally, the time to criticality is different for different instantiations of microstructure. The times to criticality ($\boldsymbol{t_c}$) obtained from all calculations in a set are

$$\boldsymbol{t_c} = (t_{c,1}, \ldots, t_{c,\xi}), \quad \xi = \text{number of instantiations}. \tag{2}$$

The data in Eq. (2) allow the cumulative probability distribution of t_c to be computed. The results are fitted to the Weibull distribution function.[33] By relating the variation of this distribution to the microstructural attributes (input parameters), we can identify relationships between the ignition sensitivity and microstructure conditions of PBXs. The distribution function can also be used to determine other statistical measures of ignition response, such as the expected mean

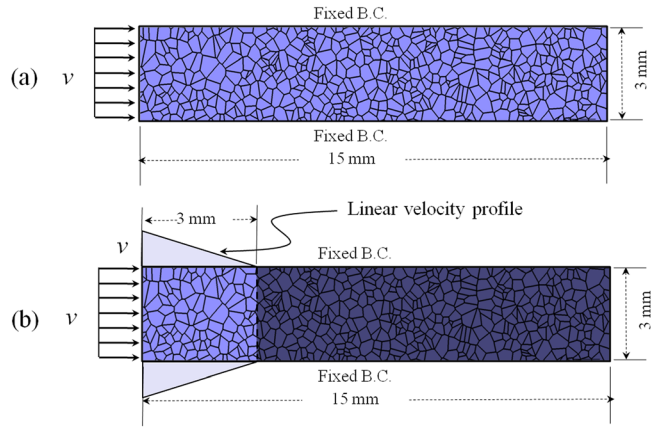

FIG. 5. Configurations for (a) transient impact loading and (b) macroscopically uniform loading without stress wave propagation.

time to criticality t_{exp}, median time to criticality t_{50} and the critical impact velocity below which no ignition occurs (v_c). These measures can be related to empirical ignition thresholds for explosives, in the form of the Walker-Wasley relation[34] and the modified James relation discussed in Ref. 33.

III. LOADING CONFIGURATIONS

Two loading configurations are used, both involve a $15\,\text{mm} \times 3\,\text{mm}$ rectangular microstructural region. This sample size is at least one order of magnitude larger than the length scale of the mean grain size for the PBX considered, giving sufficient volume representation of the microstructures.

The primary loading configuration is shown in Fig. 5(a). This configuration approximates the normal impact loading of an infinitely wide material block under conditions of macroscopic uniaxial strain. The imposed constant boundary/piston velocity approximately simulates loading under a constant input stress level. The specimen length is chosen to allow approximately the first 5.5–8.5 ms of the propagation of the stress wave from the left surface toward the right to be analyzed, before the wave arrives at the right end. This is a 2D model and the conditions of plane-strain prevail at length scales higher than the size scale of the material heterogeneities. The specimen is initially stress-free and at rest. Impact loading is effected by applying a constant normal velocity on the left end of the sample. The upper and lower boundaries are constrained such that lateral expansion (up for the upper edge and down for the lower edge) does not occur. This configuration approximates the normal impact loading of an infinitely wide material block under conditions of macroscopic uniaxial strain.

The second loading configuration is shown in Fig. 5(b). This configuration is similar to the configuration in Fig. 5(a). Used to simulate loading under a uniform state of stress without the effects of stress wave propagation, this configuration involves a linear initial particle velocity distribution over the $3\,\text{mm} \times 3\,\text{mm}$ region on the left. Other aspects of this configuration are the same as those for the loading configuration in Fig. 5(a). The prescribed initial particle velocity decreases linearly from the imposed boundary velocity v to 0 over the 3 mm length of the region. This treatment generates a macroscopically "uniform" deformation state in an average sense in the $3\,\text{mm} \times 3\,\text{mm}$ region. This configuration allows the ignition behavior to be studied for conditions of macroscopically uniform deformations, without the effects of transient stress wave propagation.

IV. RESULTS AND DISCUSSIONS

The calculations first focus on the effects of (i) impact velocity, (ii) grain volume fraction $(\eta = 0.70-0.90)$, and (iii) grain size distribution (monomodal and bimodal). For all calculations presented, the initial temperature is $T_i = 300\,\text{K}$. The boundary velocity is varied between 100 and $250\,\text{ms}^{-1}$. To illustrate the processes at hand and the stochastic treatment of the results, a representative calculation is first discussed.

The analysis is performed in two steps. First, the calculations are carried out using loading configuration 1 [see Fig. 5(a)] to allow the temperature field to evolve with time under the effects of transient stress wave propagation. Following the calculations, the threshold method described in Sec. II B is used to scan the microstructure for hotspots. Figure 6 illustrates the evolution of hotspots with time for a microstructure with a packing density of $\eta = 0.84$ in the time interval $t = 6.07$–$6.75\,\mu\text{s}$. The impact velocity is $v = 90\,\text{ms}^{-1}$. Each dot represents the detection of one hotspot with a particular combination of size and temperature. Failure mechanisms (transgranular fracture and sliding frictional heating along crack faces, intergranular interaction

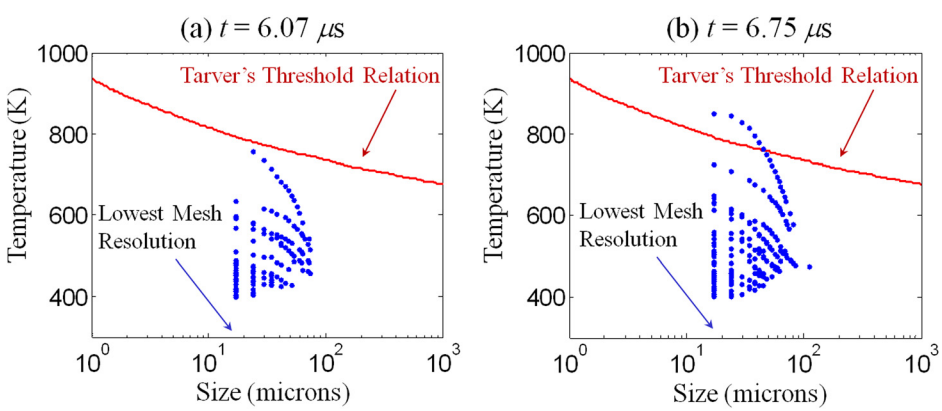

FIG. 6. Size and temperature of hotspots relative to the ignition threshold Tarver *et al.* at different times. The microstructure is that in Fig. 1(f) with $\eta = 0.84$ and the impact velocity is $v = 90\,\text{ms}^{-1}$. The size scale for the horizontal axes above is μm. This unit was inadvertently and incorrectly printed as mm in Fig. 1 of Ref. 32. The correct unit there should be μm, the same as the unit here.

and heating due to binder deformation and crack face friction) cause energy dissipation and local temperature rise. Localized temperature increases lead to the hotspots. The use of multiple threshold temperatures in the hotspot detection algorithm allows hotspots of interests in the entire temperature-size space to be identified and analyzed. Figures 6(a) and 6(b) show that, as the threshold temperature is increased, the size and density of hotspots decrease. This finding suggests that there are fewer hotspots with higher temperatures. At the highest temperature, only 1–2 hotspots exist. These hotspots are the first to reach the threshold condition for thermal criticality. Obviously, the ignition of the material is determined by a small number of hotspots in the domain analyzed. Although some hotspots in Fig. 6 appear to be close to the mesh resolution of 15 μm, it is important to point that the overall temperature fields and the temperature variations within hotspots are properly resolved with sufficient spatial resolution, as stated earlier. This situation should be viewed objectively with the proper information in mind. Hotspots have varying temperatures, as shown, e.g., in Figs. 2 and 7 in Ref. 32. Specifically, the temperature is highest at the center of a hotspot, causing a sharp spike to form at the center. As the cutoff temperature (called ΔT_{thres} in Ref. 32) is increased to identify hotspots with high temperatures, a hotspot is intersected only at the center and would appear smaller as only its central portion is included in the analysis. This accounting of the hottest central region of a hotspot should not be mistaken as the whole hotspot not having been represented by enough finite element data points spatially.

Figure 6(a) also shows the threshold of Tarver *et al.* [Eq. (1)] for thermal criticality. At $t = 6.07$ μs, no hotspot has reached any size-temperature combination required for criticality. At 6.75 μs, one hotspot has reached or crossed the threshold curve. Note that each trail of dots in the figure represents one hotspot, because hotspots have higher temperatures in the interior and the higher temperature interior has temperature-size combinations that are above the Tarver threshold as successively higher threshold temperatures are used in the analysis of each hotspot. Once the criterion outlined in Sec. II B is satisfied, the material is assumed to have reached the critical state for thermal runaway. The time (measured from the beginning of loading) at which this is taken as the time to criticality (t_c) and is obtained for different combinations of impact velocity, grain volume fraction and size distribution.

The variations in the time to criticality t_c among different samples subject to the same loading result from the variations in microstructure geometry. It is possible to generate ensembles with desired numbers of samples that share certain microstructural attributes that are similar to prescribed levels of accuracy. The microstructure attributes of initial interest in this regard are grain volume fraction and grain size distribution. The number of microstructure instantiations or the "sample set size" required for a particular analysis depends on the complexity of the problem, the parameter ranges involved and the desired level of accuracy of the statistical analysis. The complexity of the calculations is evident from the fact that the simulation of the impact response of one sample has a wall clock time of approximately one week while running on 24 computing cores on a parallel computer cluster. The microstructure space analyzed here covers volume fractions in the range of $\eta = 0.70$–0.90, with both monomodal and bimodal grain size distributions for each volume fraction level. Specifically, six microstructural settings [three volume fraction levels (0.72, 0.81, and 0.90) for monomodal grains and three volume fraction levels (0.70, 0.80, and 0.84) for bimodal grains] are considered, as discussed in Sec. II A and shown in Fig. 2. The range of impact velocity of interest is $v = 100$–$250\,\mathrm{ms}^{-1}$ and up to four different impact velocity levels (100, 150, 200, and 250) are considered for each microstructure set. The number of microstructure set and impact velocity combinations studied is $6 \times 4 = 24$.

Each of the six sets of microstructures must include multiple samples. Clearly, a higher number of instantiations in each set leads to a more accurate quantification of the probability distribution function of the ignition behavior. Wild and von Collani[35] used a sample size of 50 for their analysis of explosive sensitivity. To illustrate the effect of the sample set size on the results, an analysis is conducted with sample sets that include 10, 20, and 30 instantiations. The calculations are performed using microstructures with a packing density of $\eta = 0.81$ having a monomodal grain size distribution [representative microstructure shown in Fig. 1(b)]. The impact velocity is $v = 100\,\mathrm{ms}^{-1}$. Figure 7(a) shows the probability distributions of the time to criticality for sample sizes of 10, 20, and 30. Clearly, the overall trend and the functional relation are captured well by all three sample sizes. Based on this result, the number of instantiations for each microstructural set is chosen to be 20 from here on. The resulting total number of calculations is approximately 500.

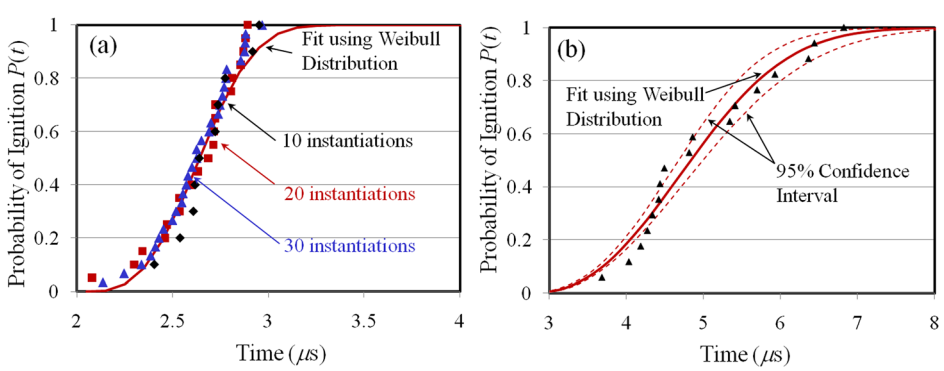

FIG. 7. (a) Probability distributions of times to criticality obtained from calculations using 10, 20, and 30 different microstructure instantiations like that in Fig. 2 with statistically similar microstructural attributes ($\eta = 0.81$, monomodal, $S_v = 16\,\mathrm{mm}^{-1}$). The impact velocity is $v = 200\,\mathrm{ms}^{-1}$. (b) Illustration of the Weibull distribution (red solid line) with the data points from calculations (black triangles). The 95% confidence interval bounds are shown using red dotted lines ($\eta = 0.70$, bimodal, $v = 100\,\mathrm{ms}^{-1}$).

A. Confidence level and confidence interval

In quantifying the safety of explosives, it is particularly important to establish confidence levels and confidence intervals for data reported. In the case of combustion in gases due to spark ignition, the 95% or 90% confidence interval is widely used in the presentation of probability estimates based on limited number of samples. For instance, Eckhoff *et al.*[36] represented the probability of ignition as a function of input energy and calculated the upper and lower limits of the probability distribution with a confidence level of 95%.

For the calculations presented in this paper, it is assumed that the distribution of the values occurs on either side of the Weibull distribution of t_c in an unbiased manner. For such a situation, the confidence interval can be computed assuming the variation to be normally distributed around the Weibull distribution. Specifically, the confidence interval for a 95% confidence level is[37]

$$t_{bound,i} = t_{c,i}(\eta, v) \pm 1.96 \frac{\sigma}{\sqrt{\xi}}, \tag{3}$$

where $t_{bound,i}$ represents the upper and lower limits of the time to ignition for the ith sample, σ is the standard deviation of the normal distribution of the variation, and ξ is the number of samples. To provide a quantitative perspective for this relation, Fig. 7(b) shows the ignition times of a set of PBX microstructures with a packing density of $\eta = 0.81$ and a monomodal size distribution of grains. The impact velocity is 200 ms^{-1}. The probability distribution of t_c is fitted to a Weibull distribution as shown by the solid line in Fig. 7(a). The confidence envelopes [shown in dotted lines in Fig. 7(a)] represent the probabilistic bounds within which 95% of the results are expected to lie.

B. Probability distribution of time to criticality

Figures 8(a)–8(f) show the probability distributions of the time to criticality t_c for microstructures with different volume fractions ($\eta = 0.72$–0.90) and grain size distributions (monomodal, bimodal). The impact velocity is in the range of $v = 100$–250 ms^{-1}. For each case, no critical hotspots are formed before a minimum cutoff time t_0. Both the minimum value and the overall distribution of the ignition time depend on microstructural attributes and loading condition.

The distribution of t_c is affected by impact velocity. In general, the time to criticality values span over a range, with lower impact velocities giving rise to wider ranges. This means that the distribution of time to criticality is more spread out at lower impact velocities, in other words, different samples show larger difference in behavior at lower

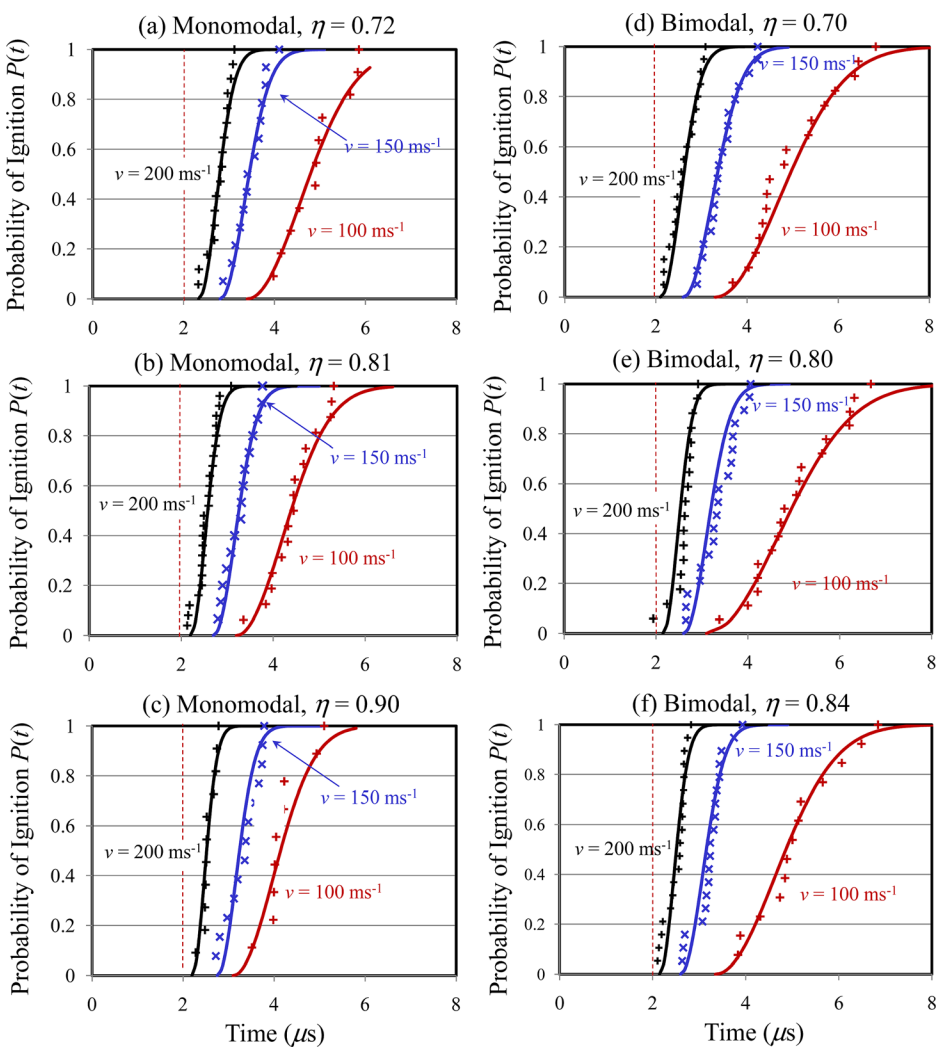

FIG. 8. Cumulative probability distributions of the time to criticality for microstructures with different grain volume fractions ($\eta = 0.72$–0.90) and grain size distributions (monomodal and bimodal) for impact velocity $v = 100$–200 ms^{-1}.

impact velocities. This observation reflects the fact that at lower impact velocities (e.g., $v \leq 100\,\mathrm{ms}^{-1}$). The stresses and rates of deformation are lower, leading to longer times for failure to occur and hotspots to evolve; as a result, hotspots are more spatially spread out and more significantly influenced by random material heterogeneities. At high impact velocities (e.g., $v > 100\,\mathrm{ms}^{-1}$), on the other hand, severe deformation and grain failure occur near the impact surface early in the loading process, dissipation and heating are the most intense near the impact face and gradually decrease toward the front of the propagating stress wave. Consequently, dominant hotspots are more concentrated near the impact surface, resulting in shorter times to criticality for hotspots less variations among different samples in term of t_c.

Figures 8(a)–8(c) show the distributions of the time to criticality for microstructures with monomodal grain size distributions. The packing density η is 0.72, 0.81, and 0.90, respectively. The corresponding results for microstructures with bimodal grain size distributions at $\eta = 0.70$, 0.80, and 0.84 are shown in Figs. 8(d)–8(f), respectively. As the packing density increases, the material becomes stiffer and generates higher levels of overall stress at the same impact velocity. Higher stresses lead to higher rates of dissipation and higher temperature increases. Consequently, the time to criticality is in general shorter at higher grain volume fractions. The distributions of t_c for the lower packing densities of $\eta = 0.72$ [Fig. 8(a)] and $\eta = 0.70$ [Fig. 8(d)] are over wider ranges compared with the distributions for the corresponding higher packing densities in Figs. 8(b) and 8(c) and Figs. 8(e) and 8(f).

Variations in the distribution of grain size also affect the sensitivity of PBX. In general, the time to criticality is more spread out for bimodal microstructures than for monomodal microstructures at the same packing density and the same load intensity [see, e.g., Figs. 8(a)–8(c) and Figs. 8(d)–8(f)]. The level of difference between the two types of microstructures depends on load intensity. At impact velocities above $150\,\mathrm{ms}^{-1}$, the difference is small and the responses for both monomodal and bimodal distributions are similar. However, at lower impact velocities ($v \leq 100\,\mathrm{ms}^{-1}$), the distributions of t_c for bimodal microstructures are spread out over much wider ranges of time than the distributions for monomodal microstructures. The average particle sizes in monomodal distributions are larger than the average particle sizes in bimodal distributions, giving rise to higher levels of heterogeneity and more significant differences in behavior among different samples in the same set. In contrast, the smaller grains in microstructures with bimodal grain size distributions can rearrange and more effectively absorb the loading to keep stresses and temperature rises lower, leading to longer times to criticality and larger variations among samples in each set. To simply put, bimodal grain distributions lead to less sensitive PBXs under otherwise identical conditions.

C. Quantification and effects of variations of microstructural attributes

Some microstructure attributes can be more easily and precisely controlled in materials design and synthesis. The overall packing density η and the average grain size are two such attributes. Other attributes are more difficult to control accurately, the distribution of grain size is one. The distributions of grain size of samples within a set of statistically similar microstructures which have, for example, the same packing density η and the same average grain size δ, may be quite different. As it turns out, the differences in grain size distribution among samples have a significant impact on the stochastic behavior of PBXs, as we will show below. For this reason, it is necessary to define a parameter (or parameters) which can be used to quantify the variations among microstructures which are statistically "similar" according to some commonly used measures (such as packing density and average grain size) but may be different in ways that can make their behaviors vary significantly from each other.

To illustrate this point, we consider the effect of the variations of grain size distribution among samples in a given microstructure set on the time to criticality. Figure 9 shows the distributions of the time to criticality for two sets of microstructures. One set has large (L) and the other has small (S) variations among the grain size distributions, as shown in Figs. 4(a) and 4(b). Specifically, the two sets of microstructures have the same grain volume fraction of $\eta = 0.81$ and the same overall average size density histograms as represented by the grey columns. The variations of grain size distribution here referred the error bars in the histograms. These error bars show the range of the grain size density among the samples in a microstructure sample set. To understand the charts, note that each of the 20 microstructure samples (or instantiations) in a set has a histogram quantifying its grain size distribution. The heights of the grey columns represent the averages of the 20 histograms and the error bars denote the maximum and minimum densities among the 20 histograms. Figure 9 shows the results for three impact velocities between 100 and $200\,\mathrm{ms}^{-1}$. At high impact velocities, the variations in the time to criticality are similar for both sets. However, at a lower velocity of $v = 100\,\mathrm{ms}^{-1}$, the two sets show similar behavior at the low end of the curves (time to

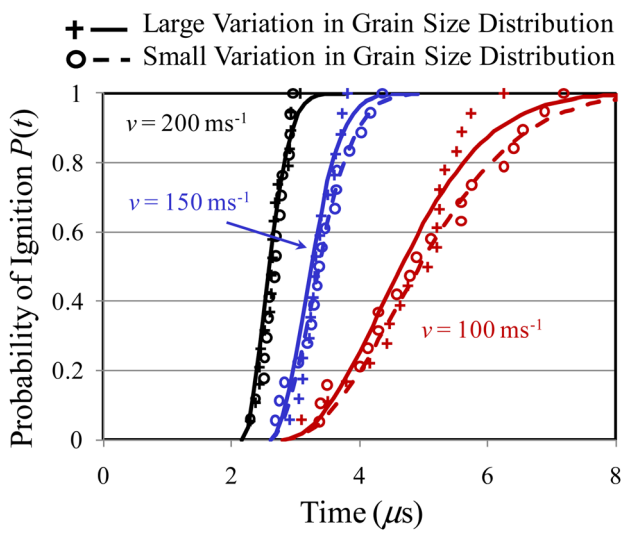

FIG. 9. Cumulative probability distributions of the time to criticality for microstructures with different levels of variations in grain size distributions for $v = 100$–$200\,\mathrm{ms}^{-1}$ ($\eta = 0.81$).

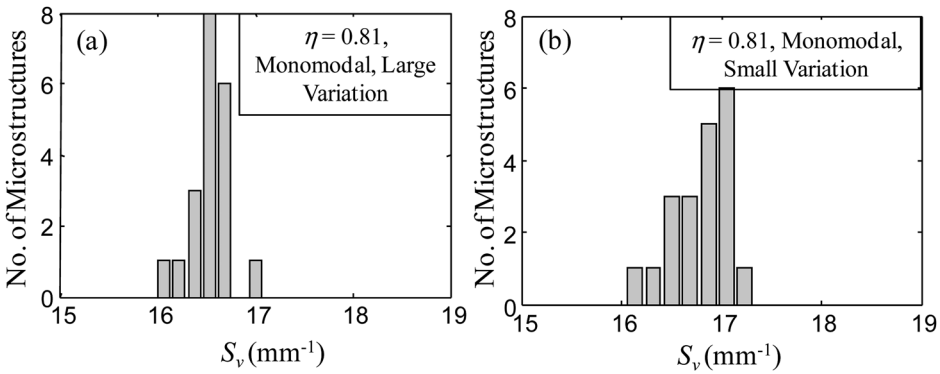

FIG. 10. Interface area per unit volume (specific interface area) for microstructures with large and small variations in grain size distributions ($\eta = 0.81$, monomodal).

criticality up to $t \sim 5\ \mu s$) but diverge at the high end ($t > 5\ \mu s$) of the curves. Specifically, the set with large variations in grain size distributions (set *L*) has a steeper profile and less variation in response than the set with smaller variations in grain size distributions (set *S*). The outcome that set *L* has larger variations among the samples but shows smaller variations in response is inconsistent with the logically expected trend. *The result suggests that the samples in the two sets of microstructures are not sufficiently similar in a statistical sense. In other words, simply having the same packing density, average grain size and average grain size distribution is not sufficient to guarantee statistical similitude of microstructures when it comes to impact-induced ignition of PBXs.*

To understand the reason, we consider the correlation between the variations in grain size distributions (shape of the histogram profiles) and the specific interfacial area (S_v) between the HMX grains and the polymer binder in the composite. Figures 10(a) and 10(b) show the distributions of S_v for the 20 samples in each of the two sets of microstructures in Figs. 4(a)–4(d). Significant differences are seen between the two histograms, i.e., there is no common trend in the profiles of S_v. It is well known that the specific interfacial area is an important parameter determining the ignition behavior of PBXs.[38,39] To properly delineate the statistical trends in behavior, more systematically constructed microstructure sample sets must be developed.

To this end, we consider the effects of both the specific surface area S_v and its statistical variation ΔS_v on the ignition response. Two sets of microstructures are presented in Fig. 11, one with a large ΔS_v of $0.3290\,\text{mm}^{-1}$ and the other with a small ΔS_v of $0.1985\,\text{mm}^{-1}$. For both sets of calculations, the microstructures have monomodal size distributions with the same packing density of $\eta = 0.81$ and the same average specific surface area, S_v of $16\,\text{mm}^{-1}$. The distributions of the time to criticality for microstructures presented in Fig. 11 are shown in Fig. 12. The impact velocity is varied between 100 and $250\,\text{ms}^{-1}$. The results in Fig. 12 show that higher values of ΔS_v correspond to higher spreads in the time to criticality. The difference in the spread of data increases as

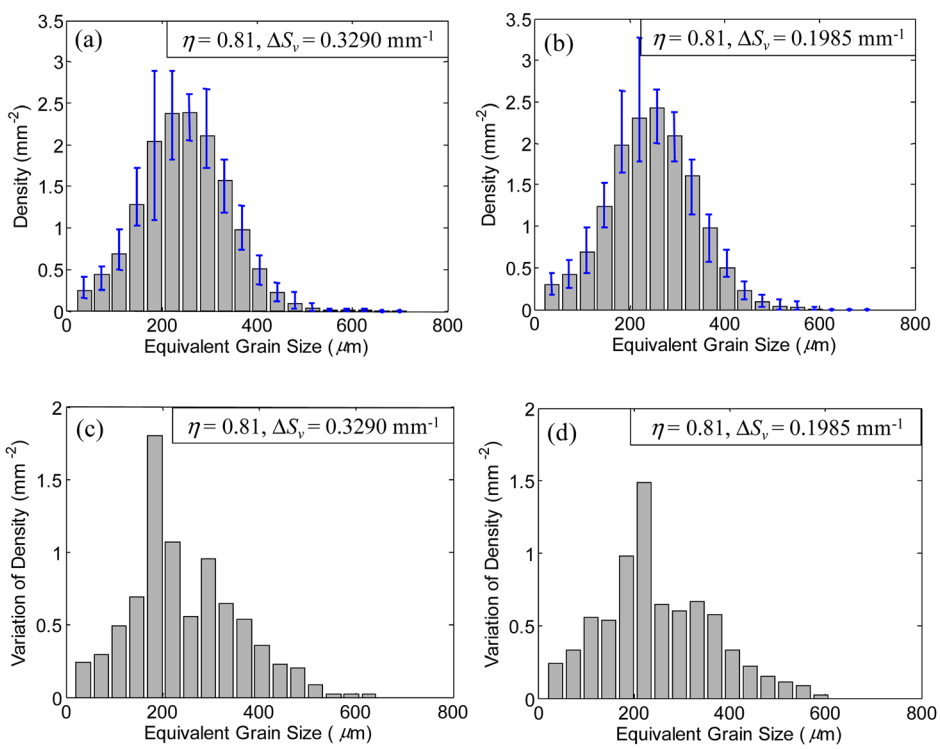

FIG. 11. Grain size distributions for microstructures having the same grain volume fraction of $\eta = 0.81$ with different variation of the specific surface area of (a) $\Delta S_v = 0.3290\,\text{mm}^{-1}$ and (b) $\Delta S_v = 0.1985\,\text{mm}^{-1}$ about the mean $S_v = 16\,\text{mm}^{-1}$. Quantification of the variations is in (c) and (d), respectively.

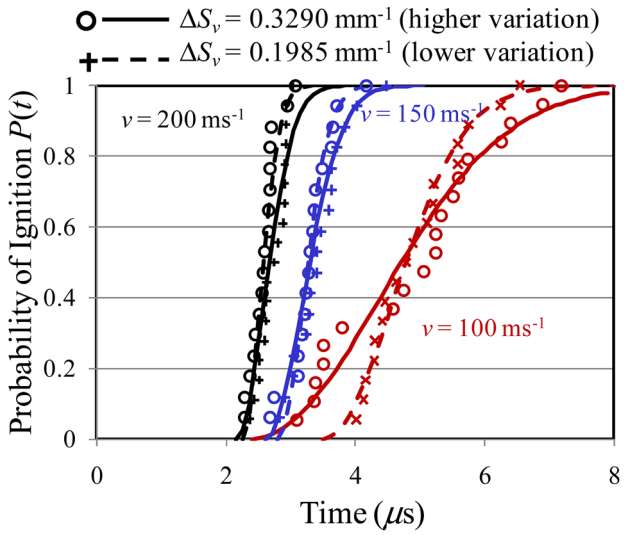

FIG. 12. Cumulative probability distributions of the time to criticality for microstructures with different variations in interface area per unit volume ($\Delta S_v = 0.1985$–$0.3290\,\text{mm}^{-1}$) for $v = 100$–$200\,\text{ms}^{-1}$.

the impact velocity decreases. Specifically, at $v = 100\,\text{ms}^{-1}$, for a ΔS_v of $0.3290\,\text{mm}^{-1}$ t_c lies between 3.0 and 7. $0\,\mu$s, whereas for a ΔS_v of $0.1985\,\text{mm}^{-1}$, t_c lies between 4 and 6.5 μs. This shows that the variations in microstructures can be reasonably well quantified by ΔS_v in the context of impact-induced ignition of PBXs. In Secs. IV F–IV H, ΔS_v is used to develop microstructure-performance scaling relationships.

D. Weibull distribution model for ignition sensitivity

Historically, the Weibull distribution[33] has been widely used in failure analysis and reliability prediction. The effect of the intensity of loading on the time to criticality can be compared to the effect of stress on the life of a mechanical component.[35] Thus, the Weibull distribution lends itself to be an excellent choice for modeling the sensitivity of explosives to impact loading. For instance, in Ref. 40 the Weibull model was applied to compare the sensitivities of RDX, HMX, pentaerythritol tetranitrate, and other popular explosives with varying grain size distributions.

Physically, critical hotspots develop only after some time has elapsed from the onset of loading. To account for this effect, a modified form of the Weibull distribution function with a lower threshold time is used. The specific form used here is[41]

$$P(t) = 1 - e^{-\Phi(t)}, \quad \Phi(t) = \begin{cases} 0, & t < t_0; \\ \left(\dfrac{t - t_0}{\tau}\right)^m, & t \geq t_0. \end{cases} \tag{4}$$

In the above expressions, $P(t)$ is the cumulative probability, t is the time to criticality, t_0 is the cutoff or threshold time below which the probability of ignition is zero, τ is a scale parameter which affects the slope of the distribution curve, and m is a shape parameter. The parameters m, τ, and t_0 together determine the Weibull distribution function [Eq. (4)] for different material and load combinations. These parameters can be related to the microstructure (packing density, grain size, grain size distribution, interfacial area per unit volume, and the statistical variations of these parameters) and impact velocity v. They can also be used to determine the threshold impact velocity v_c below which no sample in a given material set reaches thermal criticality for ignition, as we will show later. Determination of what microstructure attributes and loading intensity each of these parameters depends on and quantification of the dependence are the focus of the systematic analysis carried out in Secs. IV F–IV H. In particular, the objective is to establish explicit functional forms for the relations.

E. Physical basis for Weibull distribution model

The Weibull probability distribution function is a mathematical model independent of physical processes. The ignition of explosives is a physical process involving localized mechanical heating that is heavily affected by microstructural heterogeneity and the kinetics of chemical reactions. It is desirable to link physical mechanisms and associated variables affecting the ignition process to the model quantifying the probabilistic initiation behavior. Care needs to be taken so as to not oversimplify the problem.

To address this issue, Terao[23] and later Gilbert and Gonthier[27] used a probabilistic model to account for the stochasticity of ignition phenomena. In Terao's model, the stochasticity is accounted for by a function $\mu(t)$ which represents the probability of ignition per unit mass per unit time for a fixed amount of gas. Fundamentally for gases, μ is related to the probability of collision and subsequent reaction between molecules in a system. This probability depends on temperature T of the gas system. Terao's approach to modeling ignition in gases lends itself to the modeling of impact-induced ignition in solid high explosives. This is accomplished by accounting for the wave propagation process and temperature rise as functions of time and spatial distance from the impact surface.

Specifically for a loading event, the cumulative probability of ignition at time t is taken as $P(t)$. The inverse probability $[1 - P(t)]$ is the probability of survival or the fraction of samples not having ignited at time t. Note that $P(0) = 0$ and $P(\infty) = 1$. Now, it can be shown that the ignition probability per unit volume per unit time is[23]

$$\mu(t) = -\frac{1}{V}\frac{d[\ln(1 - P)]}{\text{dt}}, \tag{5}$$

where V is the volume of the specimen involved. For an impact-induced loading event in solid high explosive in one spatial dimension (plane loading waves), the volume of the specimen under stress increases linearly with time, that is, $V = A_c c t$, where A_c is the cross sectional area of the specimen and $c(\eta)$ is the effective wave velocity through the composite which depends on packing density η.

If a functional form of $\mu(t)V(t)$ can be determined, the explicit form of the probability distribution $P(t)$ can be obtained from the integration of Eq. (5). To identify the form of $\mu(t)V(t)$, another set of calculations is performed under

conditions of uniform loading without stress wave propagation. Although for dynamic loading, it is hard not to generate stress waves in experiments, computationally a loading configuration can be devised to create the right conditions such that no stress wave front sweeps through the material. Such a configuration uses a linearly distributed initial velocity field with $v =$ the imposed boundary velocity at $x = 0$ and $v = 0$ at $x = 3$ mm, as in loading configuration 2 in Fig. 5(b). This initial condition creates a state of nominally homogeneous uniaxial strain state over the 3 mm length of the specimen involving the initial velocity distribution. Throughout the calculation, the boundary velocity imposed at $x = 0$ is $v = 200\,\mathrm{ms}^{-1}$. The hotspot analysis focuses only on the 3 mm region, since only this region experiences the macroscopically homogenous state of stress without the influence of a propagating stress wave front. Under this condition, the volume V in Eq. (5) is the volume of the 3 mm region and is a constant which does not change with time.

Figure 13(a) shows a comparison of the probability distributions of t_c for two calculations, one uses loading configuration 1 [Fig. 5(a)] and the other uses loading configuration 2 [Fig. 5(b)]. Both cases involve an imposed boundary velocity of $v = 200\,\mathrm{ms}^{-1}$ on monomodal microstructures having a volume fraction of $\eta = 0.81$. Figure 13(b) shows the variation of $\ln[1 - P(t)]$ with the time to criticality t_c. The results are fitted to a power-law function of the form

$$\int_0^t \mu(t)V(t)dt = -\ln[1 - P(t)] = \left(\frac{t - t_0}{\tau}\right)^m. \tag{6}$$

Note that in Eq. (6), $P(t) = 0$ and $\mu(t) = 0$ when $t \le t_0$.

The fit for $\ln[1 - P(t)]$ as a function of t can be used to determine the value of m [refer to Eq. (6)]. Using Eq. (6), one can determine the probability of ignition per unit time for volume V as

$$\mu(t)V(t) = \frac{m}{\tau^m}(t - t_0)^{m-1}. \tag{7}$$

Integrating Eq. (5) along with Eqs. (6) and (7), we get

$$\int_0^P d[\ln(1 - P)] = -\frac{m}{\tau^m}\int_{t_0}^t (t - t_0)^{m-1}dt. \tag{8}$$

This yields the probability P as a function of t as

$$\ln(1 - P) = -\left(\frac{t - t_0}{\tau}\right)^m. \tag{9}$$

Equation (9) can be recast into the modified Weibull distribution in Eq. (4). This derivation shows that the Weibull distribution as a quantification for the probability of ignition is not just a numerical fit, but rather a consequence of the physics of the ignition processes whose overall probability of ignition per unit time can be described by Eq. (7).

The parameter m determines the shape of the Weibull distribution curve and hence is often referred to as the shape parameter. Tsue *et al.*[42] analyzed the ignition time in the droplet experiment using the Weibull distribution and categorized the curves into three types which correspond to $m > 1$, $m < 1$, and $m = 1$, respectively, for droplets having a constant volume. The analysis revealed that $m > 1$ is caused by driving forces for ignition that intensify with time. If $m = 1$, the onset rate of ignition is independent of time. From the fitting in Fig. 13(b), it can be seen that for the uniformly loaded case, $m = 1.28 > 1$, reflecting that fact that the temperature, and therefore the probability for ignition increases as the loading event progresses. For the case with wave propagation, $m = 2.09$, signifying a higher rate of increase of the probability for ignition resulting from the combined effects of increasing temperature (the increases of the peak and average temperatures behind the propagating wave front under non-shock loading was analyzed by Barua *et al.*[30]) and increasing volume of material involved. This value is close to the theoretical value of $m = 2$ for the special case with μ (and the overall average temperature) being constant behind the propagating wave front typically encountered during shock loading. Note that, however, for wave propagation considered here (non-shock loading), the spatial distribution of temperature is non-uniform behind the stress wave front, i.e., temperature increases are highest near the loading surface at the left end [see Fig. 5(a)] and lowest near the stress wave front (toward the right). This non-uniformity of temperature causes the density of probability of ignition to be spatially non-uniform. Consequently, $\mu(t)$ must be interpreted as the average probability of ignition per unit time per unit volume for materials behind the current stress wave front.

Figure 14 shows the values of m obtained by fitting Eq. (4) to the computationally predicted ignition times for all combinations of microstructure (monomodal and bimodal, $\eta = 0.70$–0.90) and impact velocities ($v = 100$–$250\,\mathrm{ms}^{-1}$)

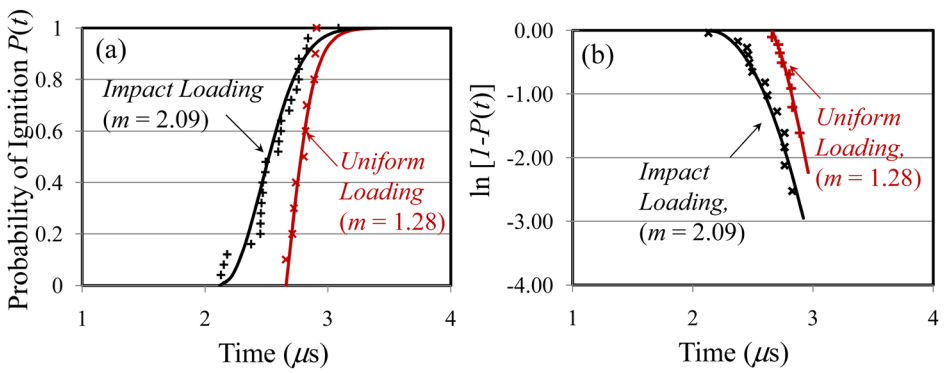

FIG. 13. Comparison of the effects of uniform and transient impact loading on the shape parameter m; (a) in P-t space and (b) in Q-t space (monomodal, $\eta = 0.81$, $v = 200\,\mathrm{ms}^{-1}$).

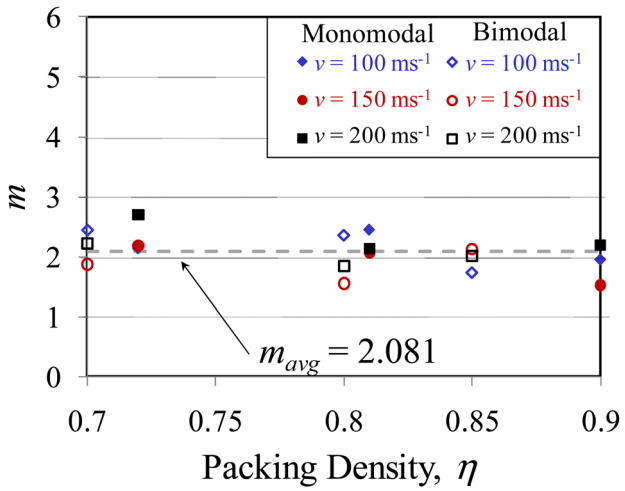

FIG. 14. Weibull parameter m as a function of grain volume fraction over a range of impact velocity ($v = 100$–$200\,\mathrm{ms}^{-1}$).

considered. The values do not change significantly with microstructural attributes or impact velocity. The average value for all calculations is 2.081. This shows that under the conditions analyzed, m is primarily dependent on the loading configuration and is not significantly influenced by microstructure or loading intensity.

F. Effect of microstructure and impact velocity on threshold time t_0

The parameter t_0 quantifies the threshold time before which no ignition is observed. Figures 15(a) and 15(b) show the values of t_0 obtained from the Weibull analysis for all cases of microstructure (monomodal and bimodal; $\eta = 0.70$–0.90) and impact velocities ($v = 100$–$250\,\mathrm{ms}^{-1}$) considered. For both monomodal and bimodal microstructures, as the boundary velocity increases, the threshold time t_0 decreases. This is expected since an increase in impact velocity leads to earlier fracture and frictional dissipation in the grains. This in turn, results in earlier formation of critical hotspots. The relationship between the threshold time and impact velocity can be quantified as

$$v^{n'} t_0 = C'(\eta), \tag{10}$$

where n' and C' are functions of packing density η and are not sensitive to the monomodal or bimodal nature of the grain size distribution. At low impact velocities, the threshold time is lower for lower packing densities. Specifically, the threshold time decreases by ~16% as the packing density increases from 0.72 to 0.90. However, at higher impact velocities, this decrease is smaller. At $200\,\mathrm{ms}^{-1}$, no significant effect of packing density on the threshold time is seen. Under the conditions analyzed, the grain size distribution does not significantly affect t_0. The values of n' and C' for the different microstructures analyzed are listed in Table II.

G. Effect of microstructure and impact velocity on scaling parameter τ

The scaling parameter τ influences the overall slope (and spread) of the probability distribution of the time to criticality t_c. Figures 16(a) and 16(b) quantify the variation of τ as a function of impact velocity in the range of $v = 100$ to $200\,\mathrm{ms}^{-1}$. The microstructures have grain volume fractions between $\eta = 0.72$ and 0.90 and different (monomodal and bimodal) size distributions. In general, τ varies with both microstructure and load intensity. For all microstructures, τ decreases (and $1/\tau$ increases) as the impact velocity increases. A higher τ corresponds to a wider range of distribution of t_c. At the same impact velocity, τ decreases as the

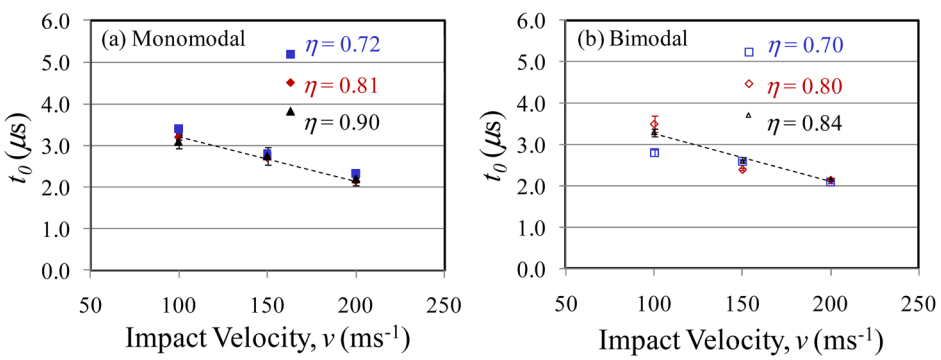

FIG. 15. Threshold ignition time t_0 as a function of grain volume fraction over a range of impact velocity ($v = 100$–$200\,\mathrm{ms}^{-1}$) for microstructures with (a) monomodal and (b) bimodal grain size distribution (the bounds show the 95% confidence intervals).

TABLE II. Parameters used in Eqs. ((8), (13), and (14)).

Microstructure	Grain volume fraction (η)	n	n'	C	C'	k	$\rho_0 c_0$ (kg m^{-2}s^{-1})
PBX – Monomodal	0.72	0.42	0.23	21.20	7.34	17.0	3.29
	0.81	0.41	0.28	19.18	8.93	15.2	3.74
	0.90	0.40	0.26	17.87	8.36	12.5	4.73
PBX – Bimodal	0.70	0.37	0.22	15.03	5.99	10.0	3.36
	0.80	0.53	0.15	31.20	4.67	18.0	3.88
	0.84	0.46	0.31	23.96	9.83	9.5	4.44

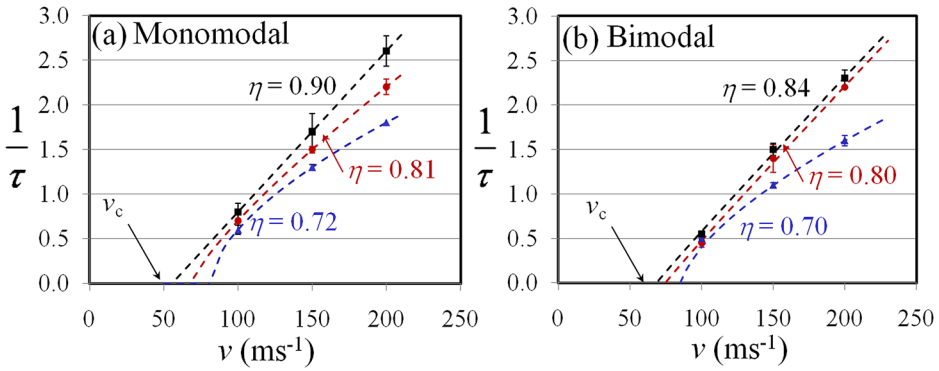

FIG. 16. Scaling parameter τ as a function of impact velocity for microstructures with a range of grain volume fractions ($\eta = 0.72$–0.90), (a) monomodal and (b) bimodal grain size distributions. The bounds show 95% confidence intervals.

grain volume fraction increases, indicating that the probability distribution of t_c narrows to a shorter time range. This is expected since higher grain volume fractions lead to higher stresses and earlier ignition, resulting in lower spreads in the probability distribution.

Grain size distribution also affects the variation of τ with v. For a particular impact velocity, τ is lower for monomodal distributions and higher for bimodal distributions. This difference is related to the fact that the range of time to ignition is higher for bimodal microstructures.

A value of $\tau = \infty$ $(1/\tau = 0)$ indicates that the probability of ignition is zero. The velocity at which this occurs (v_c) can be determined by extrapolating the curves in Figs. 16(a) and 16(b) to the horizontal axis. To obtain this critical velocity v_c, an exponential relation between τ and v is used to fit the results. This relation is of the form

$$\frac{1}{\tau} = \frac{1}{\tau_{\text{ref}}}\left(\frac{v - v_c}{v_{\text{ref}}}\right)^{\alpha}, \tag{11}$$

where τ_{ref} and v_{ref} are constants, v_c is the critical impact velocity below which no ignition is observed, and α is a fitting parameter that is a function of microstructure. The values of the constants τ_{ref} and v_{ref} are listed in Table III.

Parameter α controls the variation of $1/\tau$ with impact velocity. $1/\tau$ decreases with α when the packing density and impact velocity are fixed. A scaling law is developed to quantify α as a function of the grain volume fraction η and the variation of the specific interface area ΔS_v. The resulting relation is

$$\alpha(\eta, \Delta S_v) = \alpha_0 \eta^{2.0}\left(1 + \frac{\Delta S_v}{\Delta S_0}\right)^{-3.6}, \tag{12}$$

where α_0 and ΔS_0 are constants, as listed in Table III. This relation consists of a dimensionless term obtained by normalizing ΔS_v by reference value ΔS_0. Over the range of conditions analyzed, the specific surface area S_v does not affect α; therefore, it does not appear in Eq. (12). Overall, α increases with packing density η. It is particularly sensitive to the packing density, as indicated by the exponent of 2.0 above. This high sensitivity can be attributed to the high stresses carried by PBXs at higher packing densities.

On the other hand, α decreases as the variation of specific surface area ΔS_v increases. This decrease can be explained by the physical effect of ΔS_v. As ΔS_v increases, the probability distribution of t_c becomes more spread out, which results in lower values of $1/\tau$. This, in turn, results in lower values of α.

TABLE III. Parameters used in Eqs. ((9)–(11)).

Parameter	Units	Value
τ_{ref}	μs	1.0
v_{ref}	ms^{-1}	55.0
α_0	…	1.35
S_0	mm^{-1}	1.0
ΔS_0	mm^{-1}	20.0
v_0	ms^{-1}	21.5

H. Effect of microstructure on threshold velocity v_c

The threshold velocity v_c is the impact velocity below which no ignition is observed. The existence of a threshold velocity was proposed by James[43,44] based on the asymptotic nature of experimental data. The determination of v_c is important in design, manufacturing and transport of explosives as it relates to the safe handling limit. There have been numerous studies on low velocity impact testing of explosives.[1,2] Most of the studies on explosive survivability focus on a limited number of "go"-"no-go" experiments performed on different batches of samples. For obvious reasons, such experiments are not amenable to studying the effects of microstructure or property variation on the stochastic response of energetic composites.

The Weibull model, on the other hand, can help establish a relationship between the threshold velocity and microstructure attributes. Analyzing the variation of $1/\tau$ with v makes it possible to obtain the threshold impact velocity as the impact velocity at which $1/\tau$ goes to 0. This is done by fitting Eq. (11) to the results of calculations, yielding v_c as a function of microstructure.

Figure 17 shows the threshold velocity v_c as a function of the grain volume fraction for microstructures with both monomodal and bimodal grain size distributions. Clearly, the threshold velocity decreases as the grain volume fraction increases. This is expected since the same impact velocity induces higher overall stresses in microstructures with higher grain volume fractions. To better illustrate the trends, v_c can be expressed as a function of the grain volume fraction and the specific interface area in the form of

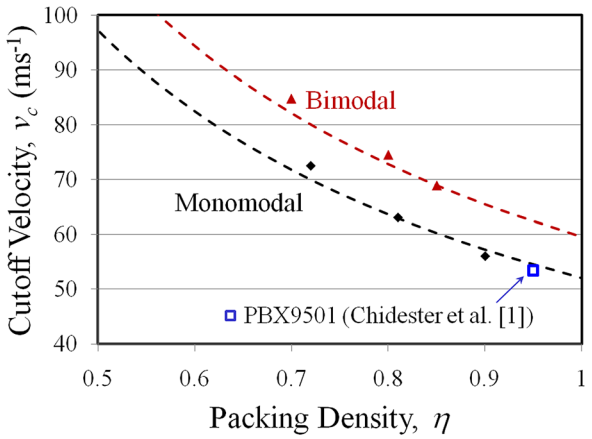

FIG. 17. Comparison of experimental threshold velocity v_c for PBX9501 and numerically predicted values as a function of grain volume fraction ($\eta = 0.70$–0.90) and grain size distributions (monomodal and bimodal).

$$v_c(\eta, S_v) = v_0 \eta^{-1.2} \left(1 + \frac{S_v}{S_0}\right)^{0.3}, \tag{13}$$

where v_0 and S_0 are constants. Here, a dimensionless term is obtained by normalizing S_v using a reference value S_0. The values of the constants in Eq. (13) are listed in Table III. Note that the variation in specific interface area (ΔS_v) does not affect the threshold impact velocity.

Equation (13) shows that a microstructure having a higher packing density is more prone to ignition and growth of reaction, provided that the specific interface area S_v is kept constant. If the two curves in Fig. 17 for monomodal and bimodal microstructures are extended to a volume fraction of 1.0, the threshold velocities for $\eta = 1.0$ can be obtained. Note that, here, the $\eta = 1.0$ case is not a single crystal, but rather a polycrystalline aggregate of HMX grains. It is well known that a single crystal of HMX is hard to ignite.[46] However, a polycrystalline solid with weak grain boundaries can fracture along grain boundaries as well as in the interior of grains, leading to extensive local frictional dissipation. Hence, a polycrystalline HMX aggregate can be highly susceptible to impact-induced ignition.

The threshold velocities for the microstructures with the bimodal grain size distributions are higher than the corresponding values for microstructures with the monomodal distribution having the same overall grain volume fraction (see Fig. 17). This reflects the fact that the specific interface area for the bimodal microstructures ($S_v \approx 25\,\text{mm}^{-1}$) is significantly higher than that for the monomodal microstructures ($S_v \approx 16\,\text{mm}^{-1}$). Equation (13) indicates that microstructures with smaller grain sizes are less susceptible to impact-induced ignition. However, a distribution with smaller grain sizes may affect other material attributes (such as strength and integrity) in different ways. Also, fine grains may give rise to smaller distances between hotspots, making detonation more homogeneous and influencing the propagation of the detonation wave. This issue is related more to the chemistry of the ignition process than to the thermo-mechanical response which is the focus of discussions here.

One way to validate the results from mesoscale calculations is to compare the predicted threshold velocity v_c with available experimental data. Using Eq. (13), we determined that the threshold velocity for a PBX with 95% HMX is between 54 and 63 ms^{-1}, depending on the grain size distribution. Chidester and coworkers[1] measured the threshold impact velocities for a variety of high explosives. Specifically, the threshold velocity for PBX9501 with a density of 1.843 g cm^{-3} was found to be approximately 53.04 ms^{-1}. Gruau *et al.*[2] reported that the minimum projectile velocity required for the ignition of PBX samples were 60–84 ms^{-1} in experiments. The range of threshold velocities obtained from our calculations correlates well with the available experimental data.

The approach outlined above for determining the threshold impact velocity is an approximation. The reason is that the threshold impact velocity obtained here is based on extrapolation of the data for higher impact velocities. A more accurate method for evaluating v_c is to run a series of calculations with successively lower impact velocities. This approach is similar to the Bruceton method.[40] However, there are two issues with this approach. The first is that it involves a large number of calculations since multiple cases need to be considered at velocities in the neighborhood of the threshold velocity. Second, a more serious issue encountered while using this approach is that at velocities near the threshold, enough time needs to be allowed for the material behind the stress wave to equilibrate. This necessitates a very large domain size and excessively long run times for the finite element calculations, even on parallel supercomputers.

I. Median time to criticality t_{50}

It is of interest to obtain some measure of the average or expected time to criticality as a function of microstructure and loading conditions. This type information is useful for comparing different types of explosives. It can also be used to validate the statistical model against well-established relations from experiments for the ignition of explosives, such as the Walker-Wasley relation[34] or the threshold relation proposed by James.[43]

Two measures of average can be estimated from the Weibull distribution. The first is the expected time to criticality t_{exp}. This measure represents the weighted mean of the time to criticality $t_{exp} = t_0 + \tau \cdot \Gamma(1 + 1/m)$, where Γ is the gamma function. An alternative measure is the time at which 50% of the samples have developed critical hotspots or the time at which the probability of ignition is $P(t_{50}) = 0.5$. This time is denoted as t_{50} and it represents the median value of the Weibull distribution. The t_{50} is a commonly used measure for quantifying the sensitivity of explosives. It is analogous to h_{50} used in drop-weight testing, which is the drop height resulting in a probability of ignition of 0.5.[47] In experiments dealing with spark ignition of gases, the criterion for defining the minimum ignition energy (MIE) is the spark energy level with a 50% probability of ignition.[48] In subsequent analyses, t_{50} is used as a measure of explosive sensitivity or susceptibility to ignition.

The Weibull distribution allows the probability distribution of the time to criticality t_c to be quantified as functions of microstructure and loading conditions. From the Weibull distribution, the median time to criticality t_{50} can be calculated as[49]

$$t_{50} = t_0 + \tau[\ln(2)]^{1/m}. \quad (14)$$

The variation of t_{50} as a function of critical impact velocity and microstructure parameters can be used to identify trends which determine ignition sensitivity in PBXs. Equation (14) allows the Weibull form to be reduced to an ignition threshold relation similar to the James relation[43] in the v-t_{50} space (see Appendix).

J. Impact velocity and median time to criticality t_{50}

The effect of grain volume fraction on the median time to criticality t_{50} is investigated using monomodal microstructures (Sec. II A). Figures 18(a) and 18(b) show the variation of t_{50} as a function of impact velocity in the range of $v = 100$ and $250\,\mathrm{ms}^{-1}$. The calculations are performed using loading configuration 1 [Fig. 5(a)]. The curves are fitted to the functional form

$$(v - v_c)^n t_{50} = C(\eta), \quad (15)$$

to illustrate the overall trends, similar to what is done in Barua *et al.*[32] The values of n and C for the different microstructures analyzed are listed in Table II. The calculation of t_{50} uses a set of 20 microstructure samples for each combination of packing density and loading condition. In general, as the impact velocity increases the time to criticality decreases. Higher grain volume fractions lead to more sensitive PBX. The variation in response with η is small at higher impact velocities and large at lower impact velocities. The diminishing effects of microstructure on response at high impact velocities reflects the fact that grain fracture occurs almost immediately upon onset of loading at high impact velocities, leading to high temperature increases in grains near the impact surface. The difference in t_{50} between the microstructures shown in Fig. 18(a) at a high impact velocity of $200\,\mathrm{ms}^{-1}$ is 0.4 μs and 1.0 μs at $100\,\mathrm{ms}^{-1}$.

Figure 18(b) compares the variations of t_{50} with impact velocity for monomodal and bimodal microstructures having the same grain volume fraction of $\eta \approx 0.80$. The calculations are performed for impact velocities between $v = 100$ and $250\,\mathrm{ms}^{-1}$. At high impact velocities ($v > 200\,\mathrm{ms}^{-1}$), t_{50} for both size distributions are similar with the monomodal distribution showing slightly higher t_{50} than the bimodal distribution. On the other hand, at lower impact velocities ($v < 200\,\mathrm{ms}^{-1}$), the monomodal microstructures have lower time to criticality and are, therefore, more susceptible to ignition than the bimodal microstructures. Specifically, at $v = 100\,\mathrm{ms}^{-1}$, the bimodal microstructures are ~20% safer than the monomodal microstructures.

K. Axial stress and median time to criticality t_{50}

The relation between axial stress (sometimes referred to as pressure, especially for shock loading) and time to criticality can provide important information regarding the key mechanisms governing ignition sensitivity. Several researchers have focused on the shock initiation threshold of PBX and GX.[24,43,50,51] For example, Hayes and Mitchell[24] explored the shock sensitivity of porous HMX and found that coarse materials are more sensitive in the low-shock pressure regime (pressure < ~5 GPa) and less sensitive in the high pressure regime. A similar effect was also observed in pressed RDX by Spear and Nanut.[39] Khasainov *et al.*[38] suggested that this shock sensitivity reversal in PBXs is due to a change in critical hotspot size resulting from differences in the specific interface area of the granules. The dependence of ignition sensitivity on input stress is a complex issue which involves two aspects: (1) the formation of critical hotspots and (2) the propagation of reaction in hotspots and associated thermal runaway. By analyzing the stress vs. time to criticality relationship from a statistical perspective using mesoscale calculations, we can address the first issue in some detail.

The distribution of stress varies significantly with time and distance from the impact face.[30] One way to characterize stress is to analyze the average stress in the loading direction across the width of the specimen. To determine the relationship between the axial stress and the median time to criticality (σ_x–t_{50} relation), the average axial stress behind the propagating wave front is used.

The effect of grain volume fraction on the relationship between σ_x and t_{50} is first investigated using monomodal microstructures (defined in Sec. II A) having grain volume fractions between $\eta = 0.70$ and 0.90. Figures 19(a) and 19(b) show the variation of t_{50} with σ_x for microstructures having

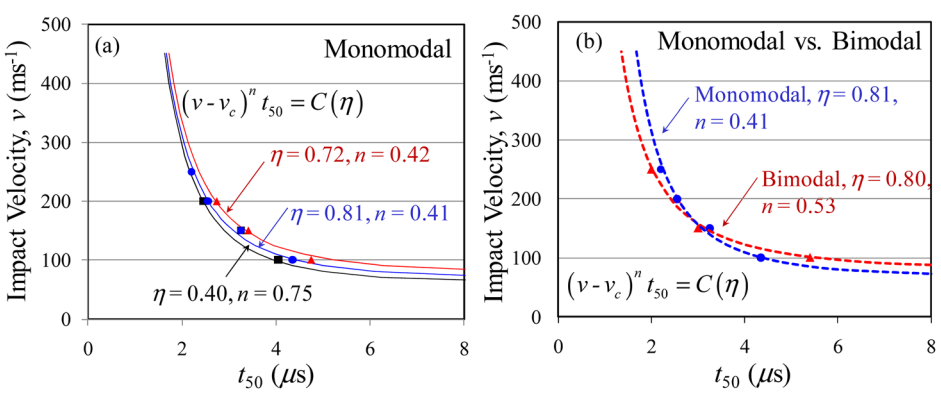

FIG. 18. Relation between impact velocity and median time to criticality for (a) microstructures with a range of initial grain volume fractions having monomodal grain size distribution, ($\eta = 0.72$–0.90, $v = 100$–200 ms^{-1}); and (b) microstructures with monomodal and bimodal grain size distributions ($\eta \sim 0.80$, $v = 100$–$200\,\mathrm{ms}^{-1}$).

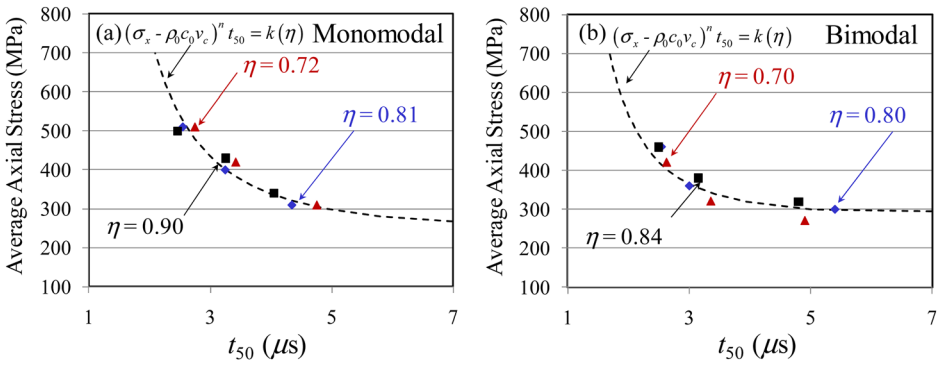

FIG. 19. Relation between average axial stress and median time to criticality for (a) microstructures with a range of initial grain volume fractions having monomodal grain size distribution, ($\eta = 0.72$–0.90, $v = 100$–$200\,\mathrm{ms}^{-1}$); and (b) microstructures with a range of initial grain volume fractions having bimodal grain size distribution, ($\eta = 0.70$–0.84, $v = 100$–$200\,\mathrm{ms}^{-1}$).

monomodal and bimodal grain size distributions for impact velocities between $v = 100$ and $200\,\mathrm{ms}^{-1}$. The calculations are performed using loading configuration 1 [Fig. 5(a)]. The curves are fitted to a functional form which can be derived from Eq. (15) as

$$(\sigma_x - \rho_0 c_0 v_c)^n t_{50} = k(\eta), \tag{16}$$

where ρ_0 is the effective density and c_0 is the effective initial longitudinal stress wave speed through the material. The values of ρ_0 and c_0 are provided in Table II. Equation (16) is similar to the relation proposed by Walker and Wasley.[34] In general, Eq. (16) provides a good fit to the results from calculations. The relation between σ_x and t_{50} collapses to a single curve for all the monomodal and bimodal microstructures analyzed, suggesting that this relation is not sensitive to the microstructural mechanisms underlying the responses of PBXs under the conditions studied. Indeed, the primary heating mechanism is fracture and friction which is heavily influenced by shear stresses as well as hydrostatic pressure. To distinguish the differences in responses, it is important to consider the deviatoric part of the stress tensor. Indeed, recent results (not shown here) suggest that the equivalent stress can be used as a measure to evaluate the effect of microstructure on the time to criticality. Specifically, high input shear stresses (equivalent stress $> \sim 0.5$ GPa) almost invariably lead to the formation of critical hotspots irrespective of the packing density. On the other hand, at lower levels of the equivalent stress, microstructures having higher packing densities have a lower time to criticality and are, therefore, more susceptible to ignition. This issue shall be the subject of a future publication.

V. CONCLUSIONS

An approach for computationally predicting and quantifying the stochasticity of the ignition process in polymer-bonded explosives under impact loading is developed. The method involves subjecting sets of statistically similar microstructure samples to identical overall loading and characterizing the statistical distribution of the ignition response of the samples. The analyses carried out in this paper have focused on the influence of random microstructure geometry variations on the critical time to ignition and the critical impact velocity below which no ignition occurs. These important quantities have been predicted based on basic material properties and microstructure attributes. Results show that the probability distribution of the time to criticality (t_c) largely follows the Weibull distribution. This probability distribution is quantified as a function of microstructural attributes including grain volume fraction, grain size, and specific binder-grain interface area along with the stochastic variations of these attributes. The relations reveal that the specific binder-grain interface area and its stochastic variation have the most influence on the critical time to ignition and the critical impact velocity below which no ignition is observed. The predicted threshold velocity v_c for ignition is consistent with available experimental data for a PBX with 95% HMX content. The v_c for a bimodal distribution of grain sizes is lower compared with that for a monomodal distribution having the same overall packing density.

Lower grain volume fractions lead to wider spreads in the distribution of the time to criticality. Microstructures having bimodal grain size distributions exhibits lower ignition sensitivity than microstructures having monomodal grain size distributions under the conditions analyzed. Finally, it is shown that the probability distribution in the Weibull form can be reduced to an ignition threshold relation similar to the James relation in the v-t space.

The study in this paper has focused exclusively on the influence of microstructure geometry variations on the critical time to ignition at given load intensity and the critical impact velocity below which no ignition occurs. It must be pointed out that the ignition response is also affected by the stochasticity in constituent properties at the microstructure level and load conditions. Those effects have not been studied. Quantification of those effects is necessary for a complete picture of the stochastic nature of ignition sensitivity of solid high explosives to emerge.

ACKNOWLEDGMENTS

The authors gratefully acknowledge support from the Defense Threat Reduction Agency (DTRA) (scientific officer: Dr. Suhithi Peiris) and the Air Force Research Laboratory (AFRL) at the Eglin AFB in Florida. Calculations are carried out on parallel computers at DPRL at Georgia Tech.

APPENDIX: DERIVATION OF CRITICALITY CONDITION FROM WEIBULL DISTRIBUTION

As mentioned Sec. IV I, the median time to criticality t_{50} can be obtained from the Weibull distribution [Eq. (4)]. The

relation between τ and v [Eq. (11)] can be substituted into Eq. (14) to obtain a relation between v and t_{50} as

$$t_{50} = t_0 + \tau_{\text{ref}} \left(\frac{v_{\text{ref}}}{v - v_c} \right)^{\alpha} [\ln(2)]^{1/m}. \quad \text{(A1)}$$

This relation can be recast into the more convenient form of

$$(v - v_c)^{\alpha}(t_{50} - t_0) = F(\eta, S_v, \Delta S_v), \quad \text{(A2)}$$

where

$$F(\eta, S_v, \Delta S_v) = \tau_{ref}(\eta, S_v, \Delta S_v) {v_{ref}}^{\alpha} [\ln(2)]^{1/m}. \quad \text{(A3)}$$

[1]S. K. Chidester, C. M. Tarver, and R. Garza, "Low amplitude impact testing and analysis of pristine and aged solid high explosives," in Eleventh (International) Symposium on Detonation, ONR (1998), 33300.

[2]C. Gruau, D. Picart, R. Belmas, E. Bouton, F. Delmaire-Sizes, J. Sabatier, and H. Trumel, "Ignition of a confined high explosive under low velocity impact," Int. J. Impact Eng. **36**, 537–550 (2009).

[3]W. Fickett and W. C. Davis, *Detonation: Theory and Experiment* (Dover Publications, 2011).

[4]B. Asay, *Non-Shock Initiation of Explosives* (Springer-Verlag Berlin Heidelberg, Berlin, Heidelberg, 2010).

[5]J. C. Foster, Jr., D. S. Stewart, and K. Thomas, "Multi-scale statistical design of high energy density materials," AIP Conf. Proc. **955**, 369 (2007).

[6]R. Engelke and S. A. Sheffield, "Initiation and propagation of detonation in condensed-phase high explosives," High-Press. Shock Compression Solids III **3**, 171 (1998).

[7]D. J. Benson and P. Conley, "Eulerian finite-element simulations of experimentally acquired HMX microstructures," Modell. Simul. Mater. Sci. Eng. **7**, 333–354 (1999).

[8]M. R. Baer, "Modeling heterogeneous energetic materials at the mesoscale," Thermochim. Acta **384**, 351–367 (2002).

[9]W. M. Trott, M. R. Baer, J. N. Castaneda, L. C. Chhabildas, and J. R. Asay, "Investigation of the mesoscopic scale response of low-density pressings of granular sugar under impact," J. Appl. Phys. **101**, 024917 (2007).

[10]R. Panchadhara and K. A. Gonthier, "Mesoscale analysis of volumetric and surface dissipation in granular explosive induced by uniaxial deformation waves," Shock Waves **21**, 43–61 (2011).

[11]A. Barua and M. Zhou, "A Lagrangian framework for analyzing microstructural level response of polymer-bonded explosives," Modell. Simul. Mater. Sci. Eng. **19**, 24 (2011).

[12]M. Zhou, "Exceptional properties by design," Science **339**, 1161–1162 (2013).

[13]S. Ye, K. Tonokura, and M. Koshi, "Energy transfer rates and impact sensitivities of crystalline explosives," Combust. Flame **132**, 240–246 (2003).

[14]S. G. Cochran, *Statistical Treatment of Heterogeneous Chemical Reaction in Shock-Initiated Explosives* (Lawrence Livermore Lab, California University, Livermore, USA, 1980).

[15]E. L. Lee and C. M. Tarver, "Phenomenological model of shock initiation in heterogeneous explosives," Phys. Fluids **23**, 2362–2372 (1980).

[16]Y. Horie, Y. Hamate, D. Greening, and T. Dey, "Reactive burn modeling of solid explosives with a statistical treatment of hot spots in two spatial dimensions," AIP Conf. Proc. **706**, 989 (2004).

[17]Y. Hamate and Y. Horie, "Ignition and detonation of solid explosives: A micromechanical burn model," Shock Waves **16**, 125–147 (2006).

[18]A. L. Nichols III and C. M. Tarver, "A statistical hot spot reactive flow model for shock initiation and detonation of solid high explosives," in Twelfth International Symposium on Detonation, Office of Naval Research, San Diego, CA, 2002.

[19]L. G. Hill, B. Zimmermann, and A. L. Nichols, III, AIP Conf. Proc. **1195**, 432–435 (2009).

[20]F. Baras, G. Nicolis, M. M. Mansour, and J. Turner, "Stochastic theory of adiabatic explosion," J. Stat. Phys. **32**, 1–23 (1983).

[21]R. V. Browning and R. J. Scammon, "Microstructural model of ignition for time varying loading conditions," in *Shock Compression of Condensed Matter-2001, Pts 1 and 2, Proceedings*, edited by M. D. Furnish *et al.*, (Amer Inst Physics, Melville, 2002), Vol. 620, pp. 987–990.

[22]M. R. Baer, D. K. Gartling, and P. E. DesJardin, "Probabilistic models for reactive behaviour in heterogeneous condensed phase media," Combust. Theory Modell. **16**, 75–106 (2012).

[23]K. Terao, *Irreversible Phenomena Ignitions, Combustion, and Detonation Waves* (Springer-Verlag, Berlin Heidelberg, Berlin, Heidelberg, 2007).

[24]D. B. Hayes and D. E. Mitchell, *Constitutive Equation for the Shock Response of Porous Hexanitrostilbene (HNS) Explosive* (Symposium on High Pressures, Paris, France, 1978).

[25]T. B. Brill and K. J. James, "Kinetics and mechanisms of thermal decomposition of nitroaromatic explosives," Chem. Rev. **93**, 2667–2692 (1993).

[26]B. F. Henson, B. W. Asay, L. B. Smilowitz, and P. M. Dickson, "Ignition chemistry in HMX from thermal explosion to detonation," in *Shock Compression of Condensed Matter-2001, Pts 1 and 2, Proceedings*, edited by M. D. Furnish *et al.*, (2002), Vol. 620, pp. 1069–1072.

[27]J. Gilbert and K. A. Gonthier, "Meso-scale computation of uniaxial waves in granular explosive-analysis of deformation induced ignition," in *50th AIAA Aerospace Sciences Meeting Including the New Horizons Forum and Aerospace Exposition* (2012), p. 12.

[28]C. M. Tarver, S. K. Chidester, and A. L. Nichols, "Critical conditions for impact- and shock-induced hot spots in solid explosives," J. Phys. Chem. **100**, 5794–5799 (1996).

[29]A. Barua, Y. Horie, and M. Zhou, "Energy localization in HMX-Estane polymer-bonded explosives during impact loading," J. Appl. Phys. **111**, 11 (2012).

[30]A. Barua, Y. Horie, and M. Zhou, "Microstructural level response of HMX–Estane polymer-bonded explosive under effects of transient stress waves," Proc. R. Soc. London, Ser. A **468**, 3725–3744 (2012).

[31]A. Barua and M. Zhou, "Computational analysis of temperature rises in microstructures of HMX-Estane PBXs," Comput. Mech. (to be published).

[32]A. Barua, S. Kim, Y. Horie, and M. Zhou, "Ignition criterion for heterogeneous energetic materials based on hotspot size-temperature threshold," J. Appl. Phys. **113**, 064906 (2013).

[33]W. Weibull, "A statistical distribution function of wide applicability," J. Appl. Mech. **18**, 293–297 (1951).

[34]F. E. Walker and R. J. Wasley, "Critical energy for shock initiation of heterogeneous explosives," Explosivstoffe **17**, 9 (1969).

[35]R. Wild and E. von Collani, "Modelling of explosives sensitivity part 2: The Weibull-Model," Econ. Qual. Control **17**, 195–220 (2010).

[36]R. Eckhoff, M. Ngo, and W. Olsen, "On the minimum ignition energy (MIE) for propane/air," J. Hazard. Mater. **175**, 293–297 (2010).

[37]G. Snedegor and W. G. Cochran, *Statistical Methods* (Iowa State University Press, 1967).

[38]B. Khasainov, B. Ermolaev, H. N. Presles, and P. Vidal, "On the effect of grain size on shock sensitivity of heterogeneous high explosives," Shock Waves **7**, 89–105 (1997).

[39]R. J. Spear and V. Nanut, "Reversal of particle size/shock sensitivity relationship at small particle size for pressed heterogeneous explosives under sustained shock loading," J. Energ. Mater. **7**, 77–114 (1989).

[40]R. Wild and E. von Collani, "Modelling of explosives sensitivity part 1: The Bruceton method," Econ. Qual. Control **17**, 113–122 (2010).

[41]Y. Li and M. Zhou, "Prediction of fracture toughness of ceramic composites as function of microstructure: I. Numerical simulations," J. Mech. Phys. Solids **61**, 472–488 (2013).

[42]M. Tsue, T. Kadota, D. Segawa, and H. Yamasaki, "Statistical analysis of onset of microexplosion for an emulsion droplet," in Symposium (International) on Combustion (1996), pp. 1629–1635.

[43]H. R. James, "An extension to the critical energy criterion used to predict shock initiation thresholds," Propellants, Explos., Pyrotech. **21**, 8–13 (1996).

[44]H. R. James, "Shock initiation thresholds for insensitive high explosives," in *Shock Compression of Condensed Matter - 2007, Pts 1 and 2*, edited by M. Elert *et al.*, (American Institute of Physics, Melville, 2007), Vol. 955, pp. 937–940.

[45]S. K. Chidester, C. M. Tarver, and C. G. Lee, "Impact ignition of new and aged solid explosives," AIP Conf. Proc. **429**, 707 (1998).

[46]J. J. Dick, "Measurement of the shock initiation sensitivity of low-density HMX," Combust. Flame **54**, 121–129 (1983).

[47]D. Preston, G. Brown, C. B. Skidmore, B. L. Reardon, and D. A. Parkinson, "Small-scale explosives sensitivity saftey testing: A departure from Bruceton," AIP Conf. Proc. **1426**, 713 (2012).

[48]Y. Ko, R. Anderson, and V. S. Arpaci, "Spark ignition of propane-air mixtures near the minimum ignition energy: Part I. An experimental study," Combust. Flame **83**, 75–87 (1991).

[49]H. Rinne, *Parameter Estimation — Maximum Likelihood Approaches*, The Weibull Distribution (CRC, Chapman and Hall, 2008), pp. 402–454.
[50]Y. Hamate, "A computational study of microstructure effects on shock ignition sensitivity of pressed RDX," AIP Conf. Proc. **955**, 923 (2007).
[51]L.-J. Wen, Z.-P. Duan, L.-S. Zhang, Z.-Y. Zhang, Z.-C. Ou, and F.-L. Huang, "Effects of HMX particle size on the shock initiation of PBXC03 explosive," Int. J. Nonlinear Sci. Numer. Simul. **13**, 189–194 (2012).
[52]N. N. Thadhani, "Shock-induced chemical reactions and synthesis of materials," Progress Mater. Sci. **37**(2), 117–226 (1993).